Weierstraß-Institut

für Angewandte Analysis und Stochastik

Leibniz-Institut im Forschungsverbund Berlin e. V.

Numerical methods for drift-diffusion models

Patricio Farrell, Nella Rotundo, Duy Hai Doan, Markus Kantner,

Jürgen Fuhrmann, Thomas Koprucki

submitted: May 18th, 2016

Weierstraß-Institut
Mohrenstr. 39
10117 Berlin
Germany
E-Mail: patricio.farrell@wias-berlin.de
nella.rotundo@wias-berlin.de
duyhai.doan@wias-berlin.de
markus.kantner@wias-berlin.de
juergen.fuhrmann@wias-berlin.de
thomas.koprucki@wias-berlin.de

1 Introduction

The semiconductor technology is undeniably one of the most important branches in modern industry. Apart from its obvious significance to our daily lives, this technology is an excellent example of a broad collaboration among various disciplines. The development of novel technologies and devices has not only been driven by engineers, but also by physicists, mathematicans and numerical analysts. On the one hand, rigorous mathematical models allow sophisticated predictions which might be difficult to observe experimentally. On the other hand, numerical simulations have the potential to optimize device designs without the costly and time-consuming development of prototypes.

In 1950, van Roosbroeck introduced the fundamental semiconductor device equations [1] as a system of three nonlinear coupled partial differential equations. They describe the semi-classical transport of free electrons and holes in a self-consistent electric field using a drift-diffusion approximation. Since then, the so-called *van Roosbroeck system* (frequently also called *drift-diffusion system*) became the standard model to describe the current flow in semiconductor devices at macroscopic scale. Typical devices modeled by these equations range from diodes and transistors to LEDs, solar cells and lasers [2, 3]. In recent years, the emergence of quantum nanostructures [4, 5, 6, 7] and organic semiconductors [8, 9, 10] has invigorated the research activities in this area.

In this chapter, we will focus on solving the van Roosbroeck system numerically. From a mathematical point of view, the challenge lies in the strong nonlinearities, the drift dominated nature of the underlying physics, the formation of internal and boundary layers as well as the need to accurately mirror qualitative physical properties such as nonnegativity of carrier densities and consistency with thermodynamical principles. The finite difference scheme invented by Scharfetter and Gummel [11] was the first to deal appropriately with most of these difficulties for charge carrier densities described by Boltzmann statistics. Later on, Fichtner, Rose and Bank [12] extented it to higher dimensions as a finite volume scheme, providing geometric flexibility. Selberherr combined a lot of these results along with his own contributions in his textbook [13] which has become one of the standard reference works in the field.

However, often the Boltzmann approximation is insufficient and one has to impose Fermi-Dirac statistics or other constitutive laws for the charge carrier densities. For this reason, we present recent attempts to generalize the Scharfetter-Gummel approach while still reflecting the physics correctly.

In order to enable readers not familiar with semiconductor simulations to quickly grasp the main points in the discretization process of the van Roosbroeck system, we start by studying a one-dimensional problem in Section 2. Even though we have to postpone some of the solid state physics to the third section, we can already introduce many key concepts of the standard finite difference ansatz proposed by Scharfetter and Gummel which we will interpret as a one-dimensional finite volume scheme.

In Section 3, we introduce the full van Roosbroeck system in higher spatial dimensions along with its physical concepts. In Section 4, we look at its numerical solution. We present the two-point flux finite volume method for the stationary case which allows to use the Scharfetter-Gummel scheme in higher dimensions and discuss its generalization to more general carrier statistics. The remaining sections are devoted to special numerical aspects: nonlinear solvers, mesh generation, time stepping, the correct computation of terminal currents and the finite element method. In the final section, we discuss generalizations of the approach and its embedding into more complex physical models.

2 How to get started: Numerical solution of the one-dimensional stationary semiconductor equations

This section serves as a quick introduction to convey the main idea behind the van Roosbroeck system and its discretization. The van Roosbroeck system consists of three equations modeling the charge carrier flow as well as the electrostatic potential distribution in a semiconductor device. However, since the physics behind these equations is rather cumbersome and the focus of this chapter are numerical methods, we will omit some of these physical details for now and start with a relatively simple 1D problem. Thus, we can highlight the key elements (and difficulties!) in the discretization of the van Roosbroeck system. This approach may appeal to newcomers to the field of optoelectronics. Experienced readers may jump directly to Section 3, where we will dive into the physical meaning of this model.

Here, we wish to model the stationary state of a one-dimensional semiconductor device consisting of a homogeneous material on an interval $\Omega = [0, L]$ with Ohmic contacts at each end. This configuration already covers the simulation of p-n and p-i-n junctions.

2.1 One-dimensional van Roosbroeck model

The one-dimensional stationary van Roosbroeck system consists of three nonlinear ordinary differential equations for the unknown electrostatic potential $\psi(x)$, the quasi Fermi potential for electrons $\varphi_n(x)$ and the quasi Fermi potential for holes $\varphi_p(x)$. It links Poisson's equation for the electric field to the continuity equations for carrier densities as follows

$$-\frac{d}{dx}\left(\varepsilon_s \frac{d}{dx}\psi\right) = q\Big(C + p(\psi, \varphi_p) - n(\psi, \varphi_n)\Big), \tag{1a}$$

$$\frac{d}{dx}j_n = \; qR(\psi, \varphi_n, \varphi_p), \tag{1b}$$

$$\frac{d}{dx}j_p = -qR(\psi, \varphi_n, \varphi_p). \tag{1c}$$

The fluxes or current densities are given by

$$j_n = -q\mu_n n(\psi, \varphi_n)\frac{d}{dx}\varphi_n \qquad \text{and} \qquad j_p = -q\mu_p p(\psi, \varphi_p)\frac{d}{dx}\varphi_p. \tag{2}$$

The electron density n and the hole density p are related to the electric potential ψ as well as the quasi Fermi potentials of electrons and holes via

$$n(\psi, \varphi_n) = N_c \exp\left(\frac{q(\psi - \varphi_n) - E_c}{k_B T}\right) \quad \text{and} \quad p(\psi, \varphi_p) = N_v \exp\left(\frac{q(\varphi_p - \psi) + E_v}{k_B T}\right). \tag{3}$$

We stress here that in (3) we have used the so-called Boltzmann approximation. In general, the exponentials will be replaced by some monotonically increasing *statistical distribution function* $\mathscr{F}$. This function will be discussed in greater detail in Section 3.

Next, we explain the constants and functions in the van Roosbroeck system. The elementary charge q and the Boltzmann constant k_B are universal constants. The (absolute) dielectric permittivity $\varepsilon_s = \varepsilon_0 \varepsilon_r$ is given as the product of the vacuum dielectric permittivity ε_0 and the relative permittivity of the semiconductor ε_r in static (low frequency) limit. The carrier mobilities μ_n and μ_p, the conduction and valence band densities of states N_c and N_v as well as the conduction and valence band-edge energies E_c and E_v are assumed to be constant even though in general they can vary with the material (for example due to abrupt or graded heterojunctions). The temperature is also assumed to be constant; in general it can be space and even time dependent. The doping profile $C = C(x)$ describes material properties and the function $R(\psi, \varphi_n, \varphi_p)$ models the recombination and generation of electron-hole pairs. The electric field $\mathbf{E}$ is determined by the derivative (in higher dimensions the gradient) of the electrostatic potential

$$\mathbf{E} = -\frac{d}{dx}\psi\,\mathbf{e}_x,$$

where $\mathbf{e}_x$ denotes the unit normal along the x axis. A more detailed discussion on the physics behind these different quantities will be given in Section 3.

In the literature, authors frequently use a different set of unknowns for the van Roosbroeck system by replacing the quasi Fermi potentials with the carrier densities n and p. However, we prefer to use the quasi Fermi potentials for several reasons: they allow to easily model abrupt or graded heterostructures and appear naturally in the thermodynamic description of the van Roosbroeck system since the negative gradients of the quasi Fermi potentials are the driving force of the currents [14]. Even mathematically they are more beautiful as they make it possible to write the whole van Roosbroeck system in a gradient form [15] consistent with the principles of nonequilbrium thermodynamics [16]. Also carrier densities as opposed to quasi Fermi potentials vary drastically in magnitude which may lead to numerical difficulties.

The system (1) needs to be supplied with boundary conditions at $x = 0$ and $x = L$. For applied external voltages U_1 and U_2, we require the Dirichlet boundary conditions at the *Ohmic contacts*, that is

$$\psi(0) = \psi_0(0) + U_1, \qquad\qquad \psi(L) = \psi_0(L) + U_2, \qquad (4a)$$
$$\varphi_n(0) = U_1, \qquad\qquad \varphi_n(L) = U_2, \qquad (4b)$$
$$\varphi_p(0) = U_1, \qquad\qquad \varphi_p(L) = U_2. \qquad (4c)$$

We discuss the meaning of the potential ψ_0 in the next section.

2.2   Thermodynamic equilibrium and local charge neutrality

The goal is to enforce that the van Roosbroeck system (1) is consistent with *thermodynamic equilibrium* which is a physical state defined by vanishing currents

$$j_n = j_p = 0 \qquad \text{implying} \qquad \varphi_0 := \varphi_n = \varphi_p = \text{const.} \qquad (5)$$

Without loss of generality, we can set $\varphi_0 = 0$. We also discuss thermodynamic equilibrium in Section 3.1. As a consequence, the three differential equations (1) reduce to the one-

dimensional nonlinear Poisson equation

$$-\frac{d}{dx}\left(\varepsilon_s \frac{d}{dx}\psi\right) = q\left(N_v \exp\left(\frac{E_v - q\psi}{k_B T}\right) - N_c \exp\left(\frac{q\psi - E_c}{k_B T}\right) + C\right). \tag{6}$$

We supply it with the Dirichlet boundary conditions (4a) for zero voltages $U_1 = U_2 = 0$. The solution of (6) with these boundary conditions is the *built-in potential* denoted with ψ_{eq}. In general, we cannot expect to find an analytic expression for ψ_{eq}.

Another important physical concept is *local charge neutrality*, characterized by a vanishing left-hand side in the Poisson equation. Combined with the equilibrium condition (5), this leads to

$$0 = q\left(N_v \exp\left(\frac{E_v - q\psi_0}{k_B T}\right) - N_c \exp\left(\frac{q\psi_0 - E_c}{k_B T}\right) + C\right) \tag{7}$$

which can be solved for ψ_0 by solving a quadratic equation and omitting the unphysical solution, yielding

$$\psi_0(x) = -\frac{E_c - E_v}{2q} - \frac{1}{2}U_T \log\left(\frac{N_c}{N_v}\right) + U_T \log\left(\frac{C(x) + \sqrt{(C(x))^2 + 4N_{\mathrm{intr}}^2}}{2N_{\mathrm{intr}}}\right) \tag{8}$$

where the intrinsic carrier density N_{intr} and the *thermal voltage* U_T are given by

$$N_{\mathrm{intr}}^2 = N_c N_v \exp\left(-\frac{E_c - E_v}{k_B T}\right) \quad \text{and} \quad U_T = \frac{k_B T}{q}. \tag{9}$$

When evaluating (8) in the finite precision of computer floating point arithmetic the argument of the logarithm may be evaluated inaccurately or actually become zero for large negative values of $C(x)$. To avoid this problem, (8) needs to be rearranged in such a way that the numerical error is minimized. This problem is a typical pitfall occurring during the implementation of the methods described in this chapter which is caused by strong nonlinearities and high density contrasts.

The potential $\psi_0(x)$ serves two purposes. In Section 2.4 it will be used to obtain an initial guess for the nonlinear iteration to solve a discretized version of (6). On the other hand, modeling (ideal) Ohmic contacts requires local charge neutrality. Hence, the boundary values in (4a) are obtained by evaluating the function ψ_0 at the contacts $x = 0$ and $x = L$. The voltage difference between the boundary values $\psi_0(0)$ and $\psi_0(L)$ is called *built-in voltage*.

2.3   Discretizing the Poisson problem

Our goal is to find a discrete solution to (1a). For this we will use the *finite volume method* which naturally preserves many important physical properties. To see this, the reader may have a quick look in the table of contents and compare the next two sections devoted to the van Roosbroeck system and its numerical solution. It will become apparent that for many aspects the continuous model and its discretized counterpart are closely related.

We discretize the interval using a (possibly) nonuniform mesh of the form
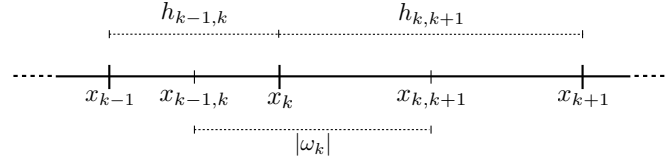
$$0 =: x_1 < \cdots < x_N := L.$$

Figure 1: 1D discretization around the kth node along with the corresponding notation.

We associate each node x_k with a *control volume* ω_k defined by the interior subintervals

$$\omega_k = \left[x_{k-1,k}, x_{k,k+1}\right] \quad \text{for} \quad k = 2, \ldots, N-1$$

and the boundary subintervals

$$\omega_1 = \left[x_1, x_{1,2}\right] \quad \text{and} \quad \omega_N = \left[x_{N-1,N}, x_N\right].$$

The boundaries of the kth control volume are given by

$$x_{k-1,k} := \frac{x_{k-1} + x_k}{2} \quad \text{and} \quad x_{k,k+1} := \frac{x_k + x_{k+1}}{2}.$$

for $k = 2, \ldots, N-1$. We point out that we have generated a disjoint partition of the the interval, $\Omega = \bigcup_{k=1}^{N} \omega_k$. This discretization along with its notation is illustrated in Figure 1.

We introduce a finite volume discretization for Poisson's equation. Using the Fundamental Theorem of Calculus, we integrate (1a) over the interior control volumes ω_k and obtain Gauss' law of electrodynamics

$$-\varepsilon_s \left(\frac{d\psi}{dx}\bigg|_{x_{k,k+1}} - \frac{d\psi}{dx}\bigg|_{x_{k-1,k}} \right) = \int_{\omega_k} q\Big(C + p(\psi, \varphi_p) - n(\psi, \varphi_n)\Big) dx. \tag{10}$$

This equation constitutes a balance law, which can be interpreted as follows: the total charge in the kth control volume is given by the difference of the electric displacement $D = -\varepsilon_s \frac{d}{dx}\psi$ at its interfaces.

So far, we have derived an integral form of Poisson's equation for every interior control volume. We need approximations of the electric displacements at the boundary of each control volume. For this we employ central finite differences:

$$\frac{d\psi}{dx}\bigg|_{x_{k,k+1}} \approx \frac{\psi_{k+1} - \psi_k}{h_{k,k+1}} \tag{11}$$

with the distance between two neighboring nodes given by

$$h_{k,k+1} := x_{k+1} - x_k.$$

Moreover, the integral over the net charge density is approximated by the rectangle method, evaluating the integrand at node x_k times the size of the control volume $|\omega_k| = x_{k,k+1} - x_{k-1,k}$. That is, the balance equation (10) is approximated by

$$-\varepsilon_s \left(\frac{\psi_{k+1} - \psi_k}{h_{k,k+1}} - \frac{\psi_k - \psi_{k-1}}{h_{k-1,k}} \right) = q\Big(C_k + p(\psi_k, \varphi_{p;k}) - n(\psi_k, \varphi_{n;k})\Big)|\omega_k|$$

or slightly rearranged

$$0 = -\varepsilon_s \left(\frac{1}{h_{k,k+1}} \psi_{k+1} - \left[\frac{1}{h_{k,k+1}} + \frac{1}{h_{k-1,k}} \right] \psi_k + \frac{1}{h_{k-1,k}} \psi_{k-1} \right) \\ - q \Big(C_k + p(\psi_k, \varphi_{p;k}) - n(\psi_k, \varphi_{n;k}) \Big) |\omega_k|,$$

(12)

where $k = 2, \ldots, N-1$. The subindices denote evaluation at a given node. So for example ψ_k means $\psi(x_k)$ as well as $\varphi_{n;k}$ indicates $\varphi_n(x_k)$. We will use this nodal notation frequently within our chapter. To incorporate the Dirichlet boundary conditions (4a), we simply impose two more equations for the endpoints, namely

$$\psi_1 = \psi_0(0) + U_1 \qquad \text{and} \qquad \psi_N = \psi_0(L) + U_2.$$

(13)

2.4   Solving the discrete nonlinear Poisson problem

Using the finite volume discretization scheme we have just described, we solve the nonlinear Poisson equation (12) with Dirichlet boundary conditions (13) in thermodynamic equilibrium ($U_1 = U_2 = 0$) to obtain the built-in potential ψ_{eq}. Recalling that there are $N-2$ interior and two boundary nodes, we end up with a system of N variables which can be summarized by the nonlinear discrete system

$$\mathbf{0} = \mathbf{F}_1(\boldsymbol{\psi}_{\text{eq}}),$$

where $\boldsymbol{\psi}_{\text{eq}} = (\psi_{\text{eq}}(x_k))_{k=1}^N$ is the vector of the nodal values. Solving this system is not straightforward due to its inherent nonlinearity. One approach to obtain a solution is Newton's method, which we discuss in more detail in Section 5. Newton's method converges quadratically – if one has a starting guess sufficiently close to the solution [17].

Solution procedure: Nonlinear Poisson problem

1. The easiest way to obtain a starting guess for the solution of (12) with Dirichlet boundary conditions (13) is to neglect the left-hand side. That is, we use the local charge neutrality condition (7) for each node, which we can solve explicitly for ψ_0 via (8). With this function we determine the components (nodal values) of our starting guess for the nonlinear Poisson problem $\boldsymbol{\psi_0}$ via

$$\boldsymbol{\psi_0} = (\psi_0(x_k))_{k=1}^N.$$

2. Solving the discrete nonlinear Poisson problem via Newton's method with the starting guess $\boldsymbol{\psi_0}$ yields the built-in potential vector solution $\boldsymbol{\psi}_{\text{eq}}$.

This solution procedure for the nonlinear Poisson equation for a p-i-n structure is illustrated in Figure 2. In the following, we address how to discretize the continuity equations. A task which turns out to be nontrivial.
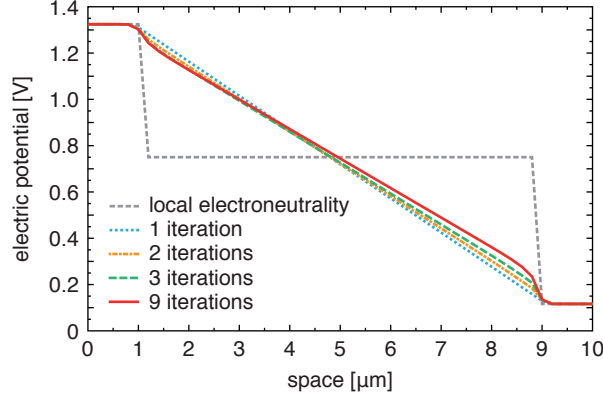
Figure 2: Convergence of the electric potential towards the thermodynamic equilibrium solution (built-in potential) for a GaAs p-i-n diode on an equidistant mesh with 51 nodes. The locally electroneutral initialization quickly converges to the built-in potential by means of a Newton iteration. The device has total length of 10 m (1 m n-doped with $N_D = 10^{16}\,\text{cm}^{-3}$, 8 m intrinsic, 1 m p-doped with $N_A = 10^{17}\,\text{cm}^{-3}$. Standard parameters for GaAs at $T = 300\,\text{K}$: $E_v = 0\,\text{eV}$, $E_c = 1.424\,\text{eV}$, $N_v = 9.0 \times 10^{18}\,\text{cm}^{-3}$, $N_c = 4.7 \times 10^{17}\,\text{cm}^{-3}$ and $\varepsilon_r = 12.9$.

2.5   Discretizing the continuity equations using the Scharfetter Gummel scheme

Now, we turn our attention to the continuity equations (1b) and (1c). We proceed just as for Poisson's equation: we integrate over the control volumes $\omega_k = [x_{k-1,k}, x_{k,k+1}]$, apply the Fundamental Theorem of Calculus for the left-hand sides and approximate the integral of the recombination term as before. For the interior control volumes we obtain

$$
\begin{aligned}
0 &= j_{n;k,k+1} - j_{n;k-1,k} - qR(\psi_k, \varphi_{n;k}, \varphi_{p;k})|\omega_k|, \\
0 &= j_{p;k,k+1} - j_{p;k-1,k} + qR(\psi_k, \varphi_{n;k}, \varphi_{p;k})|\omega_k|,
\end{aligned}
\tag{14}
$$

where $k = 2, \ldots, N-1$. Similar to before, these equations constitute a balance law in integral form which we can interpret as follows: the carrier densities within the control volume ω_k change either due to in- and outflow or by recombination effects.

The fluxes (14) need to be expressed in terms of our set of unknowns, namely the nodal values of the electrostatic and the quasi Fermi potentials. Deriving a suitable approximation for the current expressions $j_{n;k,k+1}$ and $j_{p;k,k+1}$ describing the carrier exchange between neighboring control volumes ω_k and ω_{k+1} is crucial for numerical simulations. Since standard discretization techniques such as central finite differences may lead to unphysical behavior (see Section 2.7), the derivation of such an approximation requires particular care.

For the Boltzmann approximation (3), a numerically stable scheme was invented in 1969 by Scharfetter and Gummel [11]. In fact, it has been discovered independently several times [18, 19, 20]. Its derivation is based on integrating the flux along the interval $[x_k, x_\ell]$ between two neighboring discretization nodes x_k and x_ℓ under the assumption of constant current density and constant electric field. That is, either $\ell = k-1$ or $\ell = k+1$. We illustrate the approach for the electron current density j_n.

In order to obtain a flux approximation we will make two important assumptions, namely

1. The electric field along each edge is constant. This implies that the derivative of the electric potential $\frac{d\psi}{dx}$ along the edge $[x_k, x_\ell]$ is approximated by $\frac{\psi_\ell - \psi_k}{h_{k,\ell}}$, where again $\psi_\ell = \psi(x_\ell)$ and $\psi_k = \psi(x_k)$. This is consistent with the central difference approximation for the electric field in the Poisson equation, see (11).

2. The current density j_n is assumed to be constant along the edge.

The second assumption means that the current fluxes through the boundary from one control volume to another are conserved, which implies that the derivative of the flux along the interval $[x_k, x_\ell]$ vanishes. This means that we assume that there is no recombination along the edge between neighboring nodes. Hence, we obtain for the electron flux (the hole flux follows analogously)

$$\frac{d}{dx} j_n = \frac{d}{dx} \left(-q\mu_n N_c \exp\left(\frac{q(\psi(x) - \varphi_n(x)) - E_c}{k_B T} \right) \frac{d}{dx} \varphi_n(x) \right) = 0. \tag{15}$$

We supply the differential equation with the boundary conditions

$$\varphi_n(x_k) = \varphi_{n;k} \qquad \text{and} \qquad \varphi_n(x_\ell) = \varphi_{n;\ell}. \tag{16}$$

The values $\varphi_{n;k}$ and $\varphi_{n;\ell}$ have to be determined. But for now we assume they are given. Equations (15) and (16) constitute a two-point boundary value problem. Upon integrating once and multiplication by the integrating factor

$$M(x) = \exp\left(-\frac{\psi_\ell - \psi_k}{h_{k,\ell} U_T} x \right),$$

we obtain for the integration constant $j_{n;k,\ell}$ the equation

$$j_{n;k,\ell} M(x) = q\mu_n N_c U_T \frac{d}{dx} \left(M(x) \exp\left(\frac{q(\psi(x) - \varphi_n(x)) - E_c}{k_B T} \right) \right).$$

Integrating once more from x_k to x_ℓ and using the boundary conditons (16) yields after some algebraic manipulations the Scharfetter-Gummel expression for the current flux along the edge $[x_k, x_\ell]$ between neighboring control volumes

$$j_{n;k,\ell} = j_{n;k,\ell}(\psi_k, \psi_\ell, \varphi_{n;k}, \varphi_{n;\ell}) = -\frac{q\mu_n U_T}{h_{k,\ell}} \left[B\left(-\frac{\psi_\ell - \psi_k}{U_T} \right) N_c \exp\left(\frac{q\left(\psi_k - \varphi_{n;k}\right) - E_c}{k_B T} \right) \right.$$
$$\left. - B\left(\frac{\psi_\ell - \psi_k}{U_T} \right) N_c \exp\left(\frac{q\left(\psi_\ell - \varphi_{n;\ell}\right) - E_c}{k_B T} \right) \right], \tag{17}$$

where we have introduced the *Bernoulli* function

$$B(x) = \frac{x}{\exp(x) - 1}.$$

This function smoothly interpolates between zero and $-x$, see Figure 3. Remembering the relationships (3), the flux can be brought into the simpler form

$$j_{n;k,\ell} = -\frac{q\mu_n U_T}{h_{k,\ell}} \left[B\left(-\frac{\psi_\ell - \psi_k}{U_T} \right) n_k - B\left(\frac{\psi_\ell - \psi_k}{U_T} \right) n_\ell \right]. \tag{18}$$
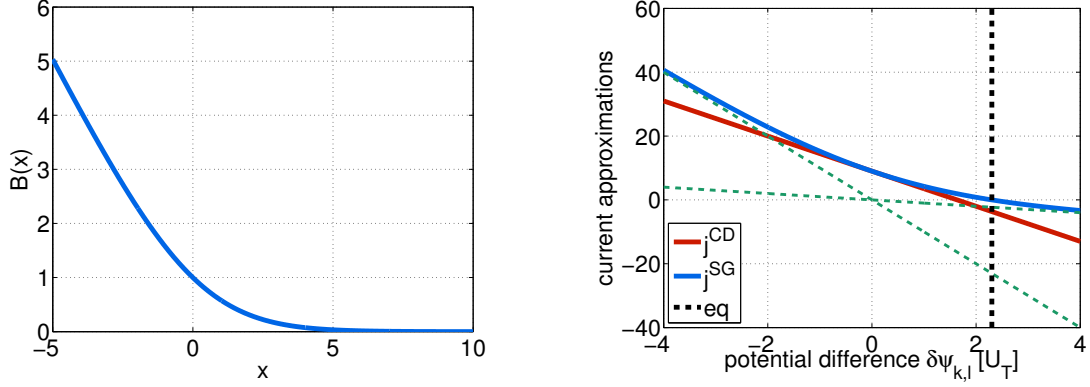
Figure 3: On the left the Bernoulli function $B(x)$ is shown. The picture on the right shows different current approximations for $q\mu_n U_T / h_{k,\ell} = 1$, $n_\ell = 10$ and $n_k = 1$ in terms of the potential difference $\delta\psi_{k,\ell}$. The dashed black line denotes the equilibrium potential difference. The green lines show the drift currents, that is the asymptotics of the Scharfetter-Gummel flux (20) for large positive and for large negative arguments. The central-difference flux is denoted with j^{CD} and the Scharfetter-Gummel flux with j^{SG}

An important property of this scheme is its consistency with the thermodynamic equilibrium. That is, similarly to (5), we have

$$j_{n;k,\ell} = 0 \quad \text{for} \quad \varphi_{n;k} = \varphi_{n;\ell} = \text{const.} \tag{19}$$

For vanishing electric fields corresponding to $\delta\psi_{k,\ell} := \psi_\ell - \psi_k = 0$, the flux $j_{n;k,\ell}$ reduces to a purely diffusive flux

$$j_{n;k,\ell} = -q\left(-D_n \frac{n_\ell - n_k}{h_{k,\ell}}\right).$$

The diffusion constant D_n is defined via the so-called *Einstein relation* $D_n = \mu_n U_T$, which we discuss in Section 3.2 in more detail. For large electric fields, we obtain asymptotically a drift flux

$$j_{n;k,\ell} = \begin{cases} -q\mu_n n_k \frac{\psi_\ell - \psi_k}{h_{k,\ell}}, & \text{for } \delta\psi_{k,\ell} \gg +U_T, \\ -q\mu_n n_\ell \frac{\psi_\ell - \psi_k}{h_{k,\ell}}, & \text{for } \delta\psi_{k,\ell} \ll -U_T. \end{cases} \tag{20}$$

These two extreme cases show that the Scharfetter-Gummel scheme naturally encompasses drift and diffusive currents depending on the strength of the local electric field, see Figure 3.

Using analogous considerations, we can derive a current expression for the holes

$$j_{p;k,\ell} = \frac{q\mu_p U_T}{h_{k,\ell}} \left[B\left(\frac{\psi_\ell - \psi_k}{U_T}\right) p_k - B\left(-\frac{\psi_\ell - \psi_k}{U_T}\right) p_\ell \right].$$

Since we have an approximation for the fluxes at the control volume boundary, we can derive from the discrete system (14) nonlinear equations for the interior nodes in terms of our set of unknowns $(\psi, \varphi_n, \varphi_p)$.

We stress once more that the previous discussion is only valid for the Boltzmann approximation made in (3). A discussion on more general distribution functions follows in Sections 3.2 and 4.2.

2.6   Solving the full discretized van Roosbroeck system

So far we have described how to derive a set of discrete and nonlinear equations from the one-dimensional van Roosbroeck system (1), namely

$$
0 = -\varepsilon_s \left(\frac{1}{h_{k,k+1}} \psi_{k+1} - \left[\frac{1}{h_{k,k+1}} + \frac{1}{h_{k-1,k}} \right] \psi_k + \frac{1}{h_{k-1,k}} \psi_{k-1} \right)
$$

$$
- q \Big(C_k + p(\psi_k, \varphi_{p;k}) - n(\psi_k, \varphi_{n;k}) \Big) |\omega_k|,
$$

$$
0 = j_{n;k,k+1}(\psi_k, \psi_{k+1}, \varphi_{n;k}, \varphi_{n;k+1}) - j_{n;k-1,k}(\psi_{k-1}, \psi_k, \varphi_{n;k-1}, \varphi_{n;k}) - qR(\psi_k, \varphi_{n;k}, \varphi_{p;k}) |\omega_k|,
$$

$$
0 = j_{p;k,k+1}(\psi_k, \psi_{k+1}, \varphi_{p;k}, \varphi_{p;k+1}) - j_{p;k-1,k}(\psi_{k-1}, \psi_k, \varphi_{p;k-1}, \varphi_{p;k}) + qR(\psi_k, \varphi_{n;k}, \varphi_{p;k}) |\omega_k|,
$$

$$
\tag{21}
$$

with $k = 2, \ldots, N-1$. For the boundary nodes x_1 and x_N, the equations are given by the boundary conditions (4):

$$
\psi_1 = \psi(0) = \psi_0(0) + U_1, \qquad \varphi_{n,1} = \varphi_n(0) = U_1, \qquad \varphi_{p,1} = \varphi_p(0) = U_1,
$$

$$
\psi_N = \psi(L) = \psi_0(L) + U_2, \qquad \varphi_{n,N} = \varphi_n(L) = U_2, \qquad \varphi_{p,N} = \varphi_p(L) = U_2.
$$

Just as for the Poisson problem we assume there are N control volumes in total. We end up with a system of $3N$ variables which we can summarize by the nonlinear discrete system

$$
\mathbf{0} = \mathbf{F}(\boldsymbol{\psi}, \boldsymbol{\varphi}_n, \boldsymbol{\varphi}_p) := \begin{pmatrix} \mathbf{F}_1(\boldsymbol{\psi}, \boldsymbol{\varphi}_n, \boldsymbol{\varphi}_p) \\ \mathbf{F}_2(\boldsymbol{\psi}, \boldsymbol{\varphi}_n, \boldsymbol{\varphi}_p) \\ \mathbf{F}_3(\boldsymbol{\psi}, \boldsymbol{\varphi}_n, \boldsymbol{\varphi}_p) \end{pmatrix},
$$

where

$$
\boldsymbol{\psi} = (\psi(x_k))_{k=1}^N, \qquad \boldsymbol{\varphi}_n = (\varphi_n(x_k))_{k=1}^N, \qquad \boldsymbol{\varphi}_p = (\varphi_p(x_k))_{k=1}^N.
$$

Again, we employ Newton's method to solve this system. We aim to guarantee an appropriate starting guess by starting from thermodynamic equilibrium where the three equation reduce to one. The solution of the full van Roosbroeck system with an applied bias is then obtained via an iteration technique which we state here.

Solution procedure: full van Roosbroeck system

1. We assume thermodynamic equilibrium (5) and set the constant quasi Fermi potentials to $\varphi_0 = 0$. With the solution procedure introduced in Section 2.4, we obtain a solution vector $\boldsymbol{\psi}_{\text{eq}}$ for the nonlinear Poisson problem with Dirichlet boundary conditions.

2. We denote with $\boldsymbol{\varphi}_n^0$ and $\boldsymbol{\varphi}_p^0$ the constant vectors, consisting of the equilibrium value for the quasi Fermi potentials, namely

$$
\boldsymbol{\varphi}_n^0 = (\varphi_0)_{i=1}^N \qquad \text{and} \qquad \boldsymbol{\varphi}_p^0 = (\varphi_0)_{i=1}^N.
$$

   We choose zero boundary voltages $U_1 = U_2 = 0$ and remember that we have obtained $\psi_0(0)$ and $\psi_0(L)$ via the charge neutrality condition. Thus we have determined the boundary conditions (4). Using the equilibrium vector $(\boldsymbol{\psi}_{\text{eq}}, \boldsymbol{\varphi}_n^0, \boldsymbol{\varphi}_p^0)$ as a new starting guess, we can now solve the full discrete system (21) with these boundary conditions via Newton's method, yielding a solution $(\boldsymbol{\psi}^1, \boldsymbol{\varphi}_n^1, \boldsymbol{\varphi}_p^1)$. That is, we compute
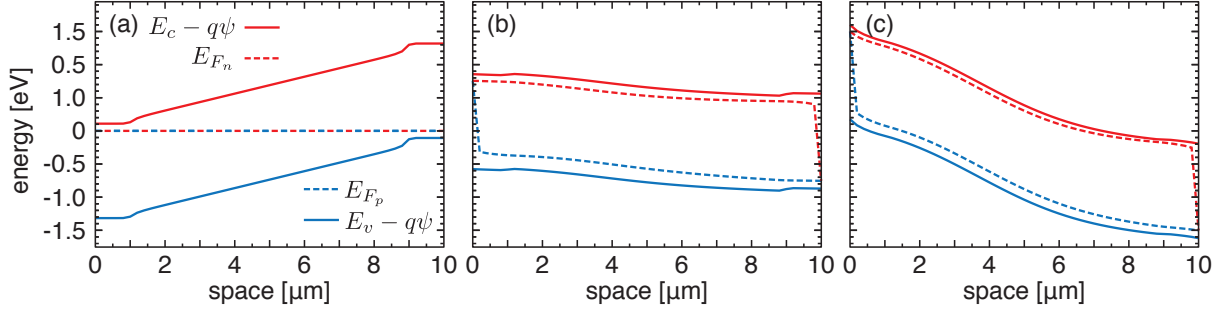
Figure 4: Computed band edge energy and quasi Fermi levels for a GaAs p-i-n diode at different values of the applied voltage. (a) Thermodynamic equilibrium (off-state, 0V), (b) $U = 1.5\,\mathrm{V}$ (flat band), (c) $U = 3.0\,\mathrm{V}$. Device has total length of 10 m (1 m n-doped with $N_D = 10^{16}\,\mathrm{cm}^{-3}$, 8 m intrinsic, 1 m p-doped with $N_A = 10^{17}\,\mathrm{cm}^{-3}$. The parameters used are standard parameters for GaAs as given in the caption of Fig. 2 and $\mu_n = 8500\,\mathrm{cm}^2\mathrm{V}^{-1}\mathrm{s}^{-1}$, $\mu_p = 400\,\mathrm{cm}^2\mathrm{V}^{-1}\mathrm{s}^{-1}$, $\tau_n = \tau_p = 1\,\mathrm{ns}$, $C_n = C_p = 1 \times 10^{-29}\,\mathrm{cm}^6\,\mathrm{s}^{-1}$ and $r_{\mathrm{spont}} = 1 \times 10^{-10}\,\mathrm{cm}^3\,\mathrm{s}^{-1}$.
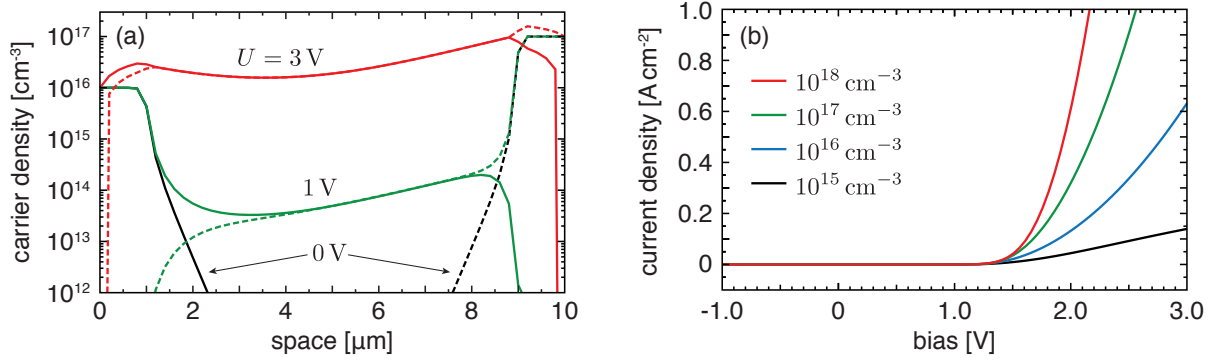

Figure 5: (a) Carrier densities in the pin-diode at different applied voltages. Electron densities are shown as solid lines, holes are illustrated by dashed lines. One observes how the intrinsic region gets populated by free carriers while increasing the applied bias. (b) Current-voltage curves for the same device with altered values of the donor density N_D. Same parameters as in Figure 4.

the equilibrium state of the full van Roosbroeck system using the equilibrium of the Poisson equation as a starting guess. We point out that solution and starting guess should agree up to machine precision by construction.

3. We slightly increase U_1 and U_2 to generate a "small" bias $\delta U = U_2 - U_1$. What small here means is not very precise and needs to be determined via trial and error. Now we solve the full discrete system (21) via Newton's method with the starting guess $(\boldsymbol{\psi^1}, \boldsymbol{\varphi_n^1}, \boldsymbol{\varphi_p^1})$ to obtain a new solution $(\boldsymbol{\psi^2}, \boldsymbol{\varphi_n^2}, \boldsymbol{\varphi_p^2})$.

4. Now we iterate the last step: gradually increase the bias and use the old solution as starting guess for the new one.

Figures 4 and 5 show the numerical results for the p-i-n structure, already introduced in Section 2.4. They depict the band edge energies, the quasi Fermi energy levels $E_{F_n} = -q\varphi_n$ and $E_{F_p} = -q\varphi_p$ as well as the carrier densities for different bias values. Additionally, the current voltage characteristics for different n-dopings are shown.
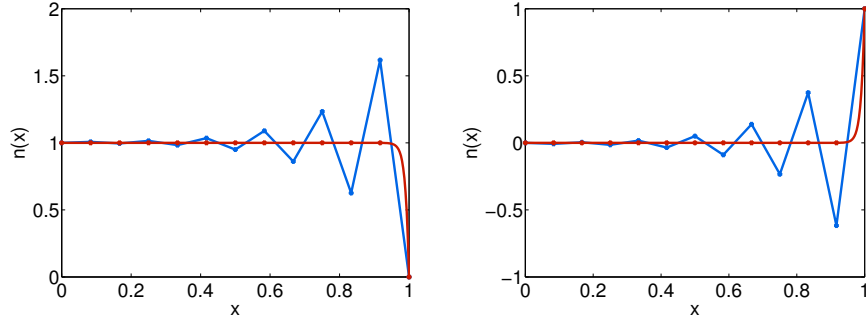
Figure 6: The exact solution (red) of (22) and its central difference approximation (blue) on a uniform mesh with mesh width $h = 1/12$. The boundary conditions (24) lead to a numerical solution which violates the maximum principle (left). On the other hand, the boundary conditions (25) produce a numerical solution which violates the positivity of the density (right). Here $qD_n = 0.01$ and $q\mu_n\delta\psi = 1$.

2.7   Why not use central finite differences for the fluxes?

Thus far, we have discussed the Scharfetter-Gummel scheme to approximate the flux at the control volume interface. One might ask why not use a simpler flux approximation, for example, central finite differences. This question we address now.

For simplicity we assume a linear electrostatic potential. In this case

$$\frac{d}{dx}\psi = \psi(1) - \psi(0) =: \delta\psi.$$

We focus on the continuity equation for electrons on the domain $\Omega = [0,1]$ which results into a linear differential equation of second order,

$$\frac{d}{dx}j_n = qD_n\frac{d^2}{dx^2}n - q\mu_n\delta\psi\frac{d}{dx}n = 0. \tag{22}$$

In this equation we have introduced the drift diffusion form of the (electron) flux

$$j_n = q\left(D_n\frac{d}{dx}n - n\mu_n\frac{d}{dx}\psi\right), \tag{23}$$

where we have used again the Einstein relation $D_n = \mu_n U_T$. We omit the physical derivation of the flux here. It is only important to know that this way of characterizing the flux is equivalent to (2).

We have already seen how to solve this type of equation numerically by solving *local* two-point boundary value problems for the flux, which yields the Scharfetter-Gummel scheme (18). Of course there are many different ways to discretize the flux (23) at a control volume interface $x_{k,\ell}$, needed in (14). For example, looking at (23) one might consider replacing the derivative of the electron density $\frac{d}{dx}n$ with a central finite difference and the density n with an average. That is, at the control volume interface we make the approximation

$$j_{n;k,\ell}^{\mathrm{CD}} = qD_n\frac{n_\ell - n_k}{h_{k,\ell}} - q\mu_n\delta\psi\frac{n_\ell + n_k}{2} = -\frac{q\mu_n U_T}{h_{k,\ell}}\left(n_k - n_\ell + \frac{\delta\psi_{k,\ell}}{U_T}\frac{n_\ell + n_k}{2}\right).$$

This, however, is a very bad idea since the scheme will become unstable, resulting under certain conditions into large oscillations. To show this, we supply (22) with two different types of boundary conditions

$$n(0) = 1 \qquad \text{and} \qquad n(1) = 0 \tag{24}$$

as well as

$$n(0) = 0 \qquad \text{and} \qquad n(1) = 1. \tag{25}$$

Then, the discretization using central finite differences shows large oscillations for $\mu_n \delta \psi / D_n = 100$, which can be seen in Figure 6. For the first boundary conditions, we can see that the *maximum principle* is violated, that is the solution exceeds both boundary values [21, 22]. For the second boundary conditions the numerically computed density becomes negative. Both observations constitute huge violations of basic physical laws and are unacceptable in applications.

The problem here is that the diffusion constant D_n is small compared to the drift constant $\mu_n \delta \psi$. We point out, that in this special one-dimensional case of vanishing recombination the Scharfetter-Gummel scheme, on the other hand, yields *exact* nodal values due to its construction. The Scharfetter-Gummel and the central difference flux are compared in Figure 3.

3   Van Roosbroeck system

In this section, we make several generalizations to the van Roosbroeck system (1). In particular, we will make the model time dependent and allow higher spatial dimensions. Before stating the equations, we discuss the physical concepts we want to encode in the model.

As in the one-dimensional case, the van Roosbroeck system consists of three equations: the Poisson equation and two continuity equations for the carrier densities. The Poisson equation describes the electric field $\mathbf{E} = -\nabla \psi$ which is generated by a scalar electric potential $\psi(\mathbf{x}, t)$ in the presence of a free charge carrier density. In a (doped) bi-polar semiconductor device, this charge density has three ingredients: the density of free (negatively charged) electrons $n(\mathbf{x}, t)$ occupying the conduction band, the density of (positively charged) holes $p(\mathbf{x}, t)$ occupying the valence band and the density of ionized built-in dopants $C(\mathbf{x}) = N_D^+(\mathbf{x}) - N_A^-(\mathbf{x})$, where N_D^+ denotes the density of singly ionized donor atoms and N_A^- is the density of singly ionized acceptor atoms.

The continuity equations (in differential form), on the other hand, model the flow of the charge carrier densities due to diffusion and drift governed by the self-consistent electric field which is generated by the net carrier density. Furthermore, the recombination and generation of electron-hole pairs influences the electron and hole densities.

The van Roosbroeck system of equations

For a bounded spatial domain $\Omega \subset \mathbb{R}^d$ where $d \in \{1, 2, 3\}$, the van Roosbroeck system consists of three coupled nonlinear partial differential equations of the form

$$-\nabla \cdot \left(\varepsilon_s \nabla \psi \right) = q \left(p - n + C \right), \tag{26a}$$

$$-q \partial_t n + \nabla \cdot \mathbf{j}_n = qR, \tag{26b}$$

$$q \partial_t p + \nabla \cdot \mathbf{j}_p = -qR, \tag{26c}$$

for $\mathbf{x} \in \Omega$ and $t \in [0, T]$. The current densities in (26b) and (26c) are given by the usual expressions

$$\mathbf{j}_n = -q\mu_n n \nabla \varphi_n \qquad \text{and} \qquad \mathbf{j}_p = -q\mu_p p \nabla \varphi_p. \qquad (26d)$$

That is, the negative gradients of the quasi Fermi potentials are the driving forces of the currents [14]. These relationships correspond directly to equations (2) in the previous section.

Within the framework of effective mass approximation [2] the densities of free carriers in a solid are given by

$$n = N_c \mathscr{F}\left(\frac{q(\psi - \varphi_n) - E_c}{k_B T}\right) \qquad \text{and} \qquad p = N_v \mathscr{F}\left(\frac{E_v - q(\psi - \varphi_p)}{k_B T}\right). \qquad (27)$$

Equations (27) indicate that the electric potential effectively leads to a bending of the energy band edge levels and thus a nonlinear, self-consistent coupling to the carrier densities is achieved. We assume a globally constant temperature for both carrier species and the crystal lattice.

The function $\mathscr{F}$ describes the occupation of energy states in the semiconductor. Since it plays an important role in the following discussion, we will define and discuss it later in Section 3.2. We only point out here that equations (27) are analogous to equations (3) when choosing for $\mathscr{F}$ the exponential function, the so-called *Boltzmann approximation*.

Initial and boundary conditions

The system (26) must be supplemented with initial and boundary conditions. The initial conditions at time $t = 0$ are given by the initial distributions ψ^I, φ_n^I and φ_p^I, i. e.

$$\psi(\mathbf{x}, 0) = \psi^I(\mathbf{x}), \qquad \varphi_n(\mathbf{x}, 0) = \varphi_n^I(\mathbf{x}), \qquad \varphi_p(\mathbf{x}, 0) = \varphi_p^I(\mathbf{x}) \quad \text{for } \mathbf{x} \in \Omega.$$

Regarding the boundary conditions, we will briefly discuss the most important case where the boundary of the domain Ω can be decomposed into Ohmic contacts, a gate contact and *artificial* interfaces, i. e.

$$\partial \Omega = \left(\bigcup_{\alpha=1}^{N_O} \Gamma_{O,\alpha}\right) \cup \Gamma_G \cup \Gamma_A.$$

Semiconductor-metal interfaces, such as Ohmic contacts, are modeled by Dirichlet boundary conditions. For any Ohmic contact $\Gamma_{O,\alpha}$ with $\alpha = 1, \ldots, N_O$, we set

$$\psi(\mathbf{x}, t) = \psi_0(\mathbf{x}) + U_\alpha(t), \qquad\qquad\qquad\qquad (28a)$$
$$\varphi_n(\mathbf{x}, t) = U_\alpha(t), \qquad\qquad \text{for all } \mathbf{x} \in \Gamma_{O,\alpha} \text{ and } t \in [0, T] \qquad (28b)$$
$$\varphi_p(\mathbf{x}, t) = U_\alpha(t), \qquad\qquad\qquad\qquad\qquad (28c)$$

where U_α denotes the corresponding externally applied contact voltage. The value ψ_0 at the boundary is defined by local charge neutrality similar to (7), where the exponential is now replaced by $\mathscr{F}$:

$$0 = N_v \mathscr{F}\left(\frac{E_v - q\psi_0(\mathbf{x})}{k_B T}\right) - N_c \mathscr{F}\left(\frac{q\psi_0(\mathbf{x}) - E_c}{k_B T}\right) + C(\mathbf{x}).$$

We just remark, that in general, this equation yields no analytical solution, and therefore its solution needs to be obtained by a nonlinear solver. The boundary conditions for

the more advanced nonlinear semiconductor-metal interfaces (Schottky contacts) can be found in [13].

Gate contacts are modeled by Robin boundary conditions for the electrostatic potential and homogeneous Neumann boundary conditions for the quasi Fermi potentials

$$\varepsilon_s \nabla \psi(\mathbf{x},t) \cdot \boldsymbol{v} + \frac{\varepsilon_{\text{ox}}}{d_{\text{ox}}}(\psi(\mathbf{x},t) - U_G(t)) = 0,$$
$$\mathbf{j}_n(\mathbf{x},t) \cdot \boldsymbol{v} = \mathbf{j}_p(\mathbf{x},t) \cdot \boldsymbol{v} = 0, \qquad \text{for all } \mathbf{x} \in \Gamma_G \text{ and } t \in [0,T], \qquad (29)$$

where ε_{ox} and d_{ox} are the absolute dielectric permittivity and the thickness of the oxide, respectively. The function $U_G(t)$ is the applied voltage at the outside of the insulating gate oxide at Γ_G.

On the remaining (artificial) interfaces one typically imposes homogeneous Neumann boundary conditions (natural boundary conditions), namely

$$\nabla \psi(\mathbf{x},t) \cdot \boldsymbol{v} = \mathbf{j}_n(\mathbf{x},t) \cdot \boldsymbol{v} = \mathbf{j}_p(\mathbf{x},t) \cdot \boldsymbol{v} = 0 \qquad \text{for all } \mathbf{x} \in \Gamma_A \text{ and } t \in [0,T]. \qquad (30)$$

Here $\boldsymbol{v}$ denotes the outer normal vector on the interface.

Recombination processes

The net recombination rate R on the right-hand side of equations (26b) and (26c) describes the radiative and non-radiative generation or recombination of carriers due to thermal excitation and various scattering effects. We assume that the recombination rate $R(n,p)$ is given by the sum of the most common processes, namely the Shockley-Read-Hall recombination R_{SRH}, the spontaneous radiative recombination R_{rad} and the Auger recombination R_{Auger}. All of these rates are of the form

$$R(n,p) = r(n,p)np\left(1 - \exp\left(\frac{q\varphi_n - q\varphi_p}{k_B T}\right)\right), \qquad (31)$$

where $r(n,p)$ is a model-dependent generation-recombination rate [2, 13, 23]. In Figure 7, one finds the definitions of these rates together with a schematic illustration of the corresponding processes. For Boltzmann statistics, (31) is equivalent to the widely used $R(n,p) = r(n,p)(np - N_{\text{intr}}^2)$, where N_{intr} is the intrinsic carrier density defined in (9).

3.1 Thermodynamic equilibrium

The thermodynamic equilibrium is characterized by vanishing current fluxes $\mathbf{j}_n(\mathbf{x},t) = \mathbf{j}_p(\mathbf{x},t) = \mathbf{0}$. As a consequence, $R(n,p) = 0$ and the quasi Fermi potentials assume constant values which due to (31) are equal:

$$\varphi_0 := \varphi_n = \varphi_p = \text{const.}$$

Without loss of generality, we set $\varphi_0 = 0$. Therefore, the van Roosbroeck system (26) reduces to the nonlinear Poisson equation

$$-\nabla \cdot \varepsilon_s \nabla \psi = q\left(N_v \mathscr{F}\left(\frac{E_v - q\psi}{k_B T}\right) - N_c \mathscr{F}\left(\frac{q\psi - E_c}{k_B T}\right) + C\right). \qquad (32)$$

We supply it with Dirichlet boundary conditions (28a) for zero voltages $U_\alpha = 0$ for $\alpha = 1,\dots,N_O$ and homogeneus Neumann boundary conditions elsewhere (30). The solution of (32) with these boundary conditions defines the *built-in potential* denoted with ψ_{eq}.
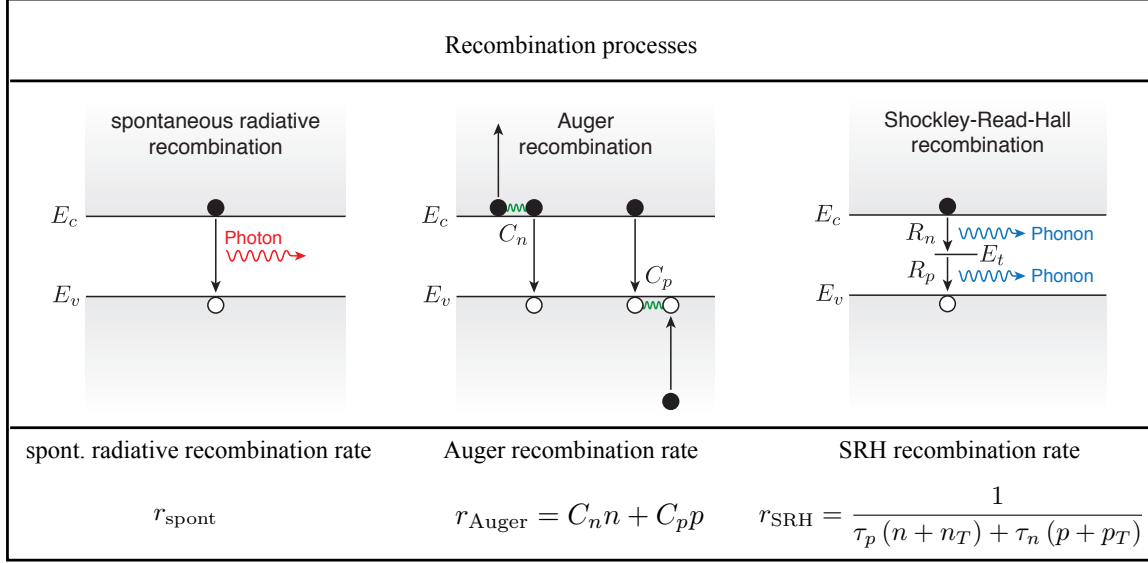
Figure 7: This figure illustrates three different recombination processes. The carrier life times τ_n, τ_p, the reference carrier densities n_T, p_T and the coefficients r_{spont}, C_n, C_p are material dependent parameters.

3.2 Non-Boltzmann statistics and generalized Einstein relation

Now, we address the statistical distribution function $\mathscr{F}$ which appears in both equations in (27). It describes the relationship between the density of the free carriers as well as the electrostatic potential and the quasi Fermi potentials [2].

Assuming that the electrons in the conduction band are in quasi equilibrium, i. e. they are described by the quasi Fermi level E_{F_n}, the electron density can be introduced as a convolution integral of the density of states $\text{DOS}(E)$ with the Fermi-Dirac distribution function

$$n = \int_{-\infty}^{\infty} \text{DOS}(E) \frac{1}{\exp\left(\frac{E - E_{F_n}}{k_B T}\right) + 1} dE. \tag{33}$$

It is possible to express this convolution as a product of the effective density of states N_c and a nondimensionalized statistical distribution function $\mathscr{F}$, i. e.

$$n(\eta) = N_c \mathscr{F}(\eta). \tag{34}$$

We consider organic and inorganic semiconductors. For inorganic, 3D bulk semiconductors with parabolic bands the statistical distribution function is given by the Fermi-Dirac integral of order 1/2 [2], which can be approximated by Blakemore [24] or Boltzmann distribution in the low density limit. For organic semiconductors it is given by the Gauss-Fermi integral [10], which reduces to a Boltzmann type of distribution function (up to some normalizing factor) in the low density limit or a Blakemore distribution function for vanishing variance σ. The latter corresponds to a δ-shaped density of states [10, 25], describing a single transport level. See Figure 8 for definitions and a relationship between these functions and Figure 9 for a graphical representation.

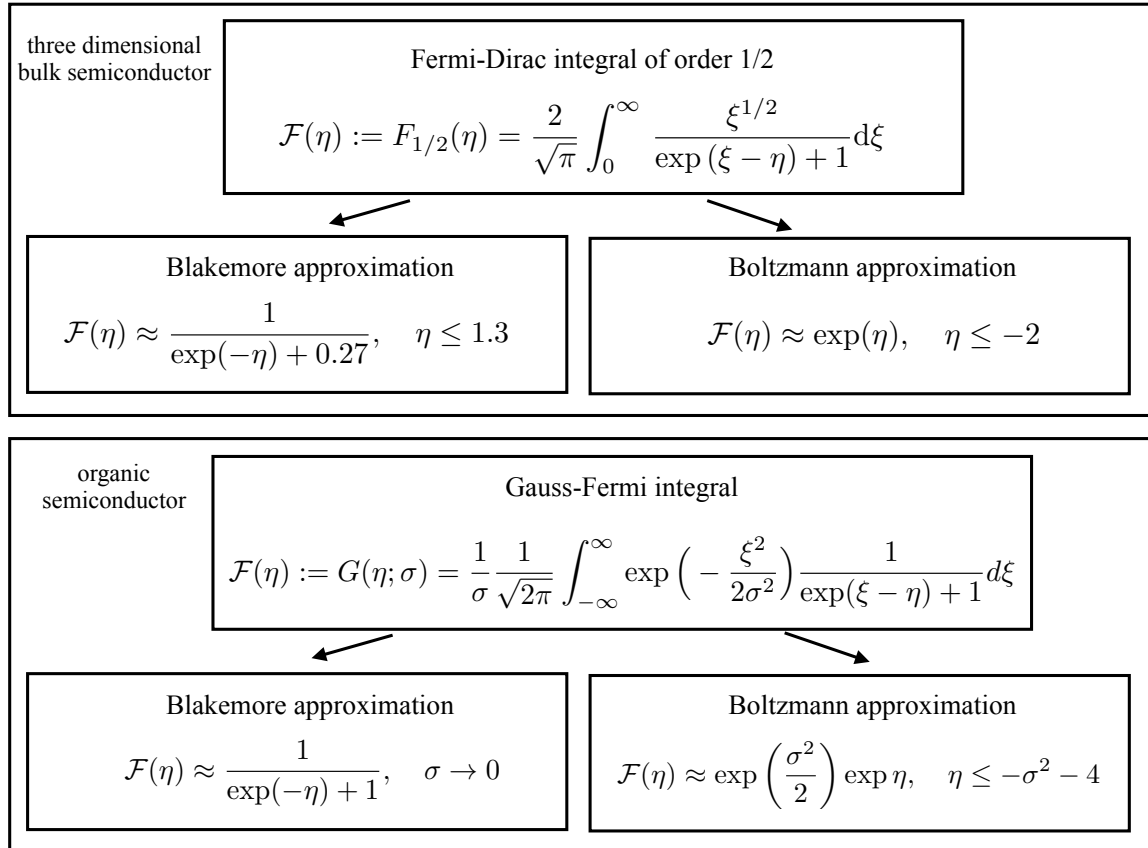For inorganic, 3D bulk semiconductors assuming parabolic bands with effective mass

Figure 8: This figure shows two important choices of the statistical distribution function: for three dimensional bulk semiconductors and for organic semiconductors [10] described by a Gaussian density of states with variance σ. Both can be approximated using the Blakemore or Boltzmann distribution function.
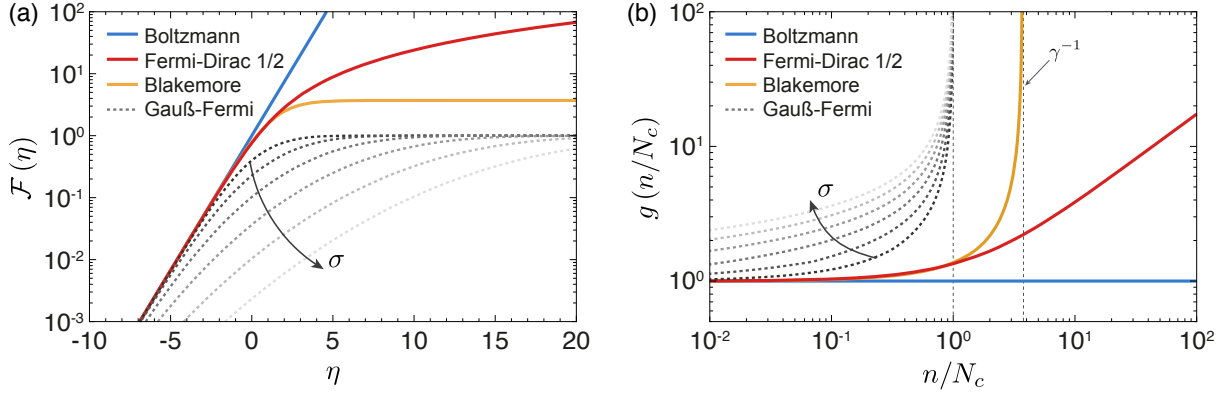
Figure 9: (a) Some frequently considered distribution functions for the density of free carriers. For the Blakemore and the Gauß-Fermi functions one obtains a saturation of the carrier density at high values of η. (b) Illustration of the diffusion enhancement factors for the distribution functions shown in (a). In the case of the Blakemore and the Gauß-Fermi functions the saturation values of the carrier density directly lead to a divergent behaviour of the nonlinear diffusion factor.

m_e^* the band-edge density of states is given by

$$N_c = 2 \left(\frac{m_e^* k_B T}{2\pi \hbar^2} \right)^{3/2},$$

where T is the temperature and $\hbar$ is the Planck constant. For organic semiconductors, the effective density of states N_c is given by the density of transport states N_t.

Introducing a general relationship between carrier density as well as quasi Fermi and electrostatic potential via (34) or rather (27), has quite a few implications. The nonlinear Poisson equation (32) becomes more complicated. In Section 2.4, we have studied how to design useful starting guesses for the Boltzmann approximation. For general distribution functions $\mathscr{F}$, it is no longer possible to obtain an explicit expression for ψ_0, like we have achieved in (8). One rather needs to solve a nonlinear equation, for example, via Newton's methods at a given point $\mathbf{x}$. For highly doped regions, the Boltzmann approximation strongly overestimates the carrier densities if $\eta > 0$, see Figure 9. This implies that the more realistic Fermi-Dirac distribution leads to a higher built-in voltage. Moreover, from a numerical point of view the Scharfetter-Gummel method needs to be adjusted. We discuss this in Section 4.2.

Finally, the distribution function $\mathscr{F}$ influences the ratio between diffusion and drift. To see this, we write the currents in *drift-diffusion* form. Using the relations for the carrier densities (27), we obtain

$$\mathbf{j}_n = -q\mu_n n \nabla \psi + q D_n \nabla n, \qquad \mathbf{j}_p = -q\mu_p p \nabla \psi - q D_p \nabla p.$$

The diffusion coefficients D_n and D_p are connected to the carrier mobilities by a *generalized* Einstein relation

$$\frac{D_n}{\mu_n} = \frac{k_B T}{q} g\left(\frac{n}{N_c}\right), \qquad \frac{D_p}{\mu_p} = \frac{k_B T}{q} g\left(\frac{p}{N_v}\right) \tag{35}$$

with a density dependent nonlinear factor

$$g(\xi) = \xi \left(\mathscr{F}^{-1} \right)'(\xi),$$

leading in general to a nonlinear diffusion coefficient. For the Boltzmann approximation, we immediately see that $g(\xi) = 1$, which gives the classical Einstein relation $D_n = q\mu_n/(k_B T)$. For non-exponential distribution function and $\xi \geq 1$, however, we note $g(\xi) \geq 1$, see [26]. For this reason, we call this factor *diffusion enhancement* as proposed in [27]. The dependence of the diffusion enhancement g on the density is depicted in Figure 9 for various distribution functions.

3.3 Free energy and dissipation rate

We consider consistency with fundamental principles of thermodynamics to be a quality measure for models describing natural processes. So it is of significant interest to study the consistency for both continuous and discretized models. Due to our simplifying assumption of constant temperature we cannot have energy conservation in the proper sense. The second law of thermodynamics for nonequilibrium processes [16, 28] requires non-negativity of the local entropy production which, multiplied by the temperature T, gives the *dissipation rate*.

For the sake of readability, we discuss these concepts for Boltzmann statistics [29] here. See [30] and [31] for more general statistics. For a triple (ψ, n, p) and a thermodynamic equilibrium solution $(\psi_{\mathrm{eq}}, n_{\mathrm{eq}}, p_{\mathrm{eq}}) := (\psi_{\mathrm{eq}}, n(\psi_{\mathrm{eq}}), p(\psi_{\mathrm{eq}}))$ of the full van Roosbroeck system the *free energy* is defined as

$$
\begin{aligned}
\mathbb{F}(\psi, n, p) = k_B T \int_\Omega & \left(n \log \frac{n}{n_{\mathrm{eq}}} - n + n_{\mathrm{eq}} + p \log \frac{p}{p_{\mathrm{eq}}} - p + p_{\mathrm{eq}} \right) d\mathbf{x} \\
& + \int_\Omega \frac{\varepsilon_s}{2} \left| \nabla \left(\psi - \psi_{\mathrm{eq}} \right) \right|^2 d\mathbf{x} + \frac{1}{2} \int_{\Gamma_G} \frac{\varepsilon_{\mathrm{ox}}}{d_{\mathrm{ox}}} \left(\psi - \psi_{\mathrm{eq}} \right)^2 ds.
\end{aligned}
\tag{36}
$$

For a transient solution $(\psi(t), n(t), p(t))$ of (26), the function $\mathbb{L}(t) = \mathbb{F}(\psi(t), n(t), p(t))$ decays exponentially as t tends to infinity and one has

$$\mathbb{L}(t) = \mathbb{L}(0) - \int_0^t \mathbb{D}(\tau) d\tau,$$

where $\mathbb{D}(t)$ is the nonnegative dissipation rate [29]

$$\mathbb{D}(t) = -\frac{d}{dt}\mathbb{L} = \int_\Omega \left(q\mu_n n |\nabla \varphi_n|^2 + q\mu_p p |\nabla \varphi_p|^2 + k_B T R \log \left(\frac{n}{n_{\mathrm{eq}}} \frac{p}{p_{\mathrm{eq}}} \right) \right) d\mathbf{x} \geq 0 \tag{37}$$

depending on t via the time evolution of n, p. This result confirms the consistency with the second law of thermodynamics. Incidentally, the function $\mathbb{L}$ is a Lyapunov function, allowing in certain situations to prove the global stability of the thermodynamical equilibrium. Furthermore, it can be used as a tool to prove uniqueness of solutions to the system (26). This leads us naturally to the following subsection.

3.4 Existence and uniqueness results

When modeling complex physical phenomena, it is often necessary to simplify the underlying physical model. Therefore, a sound mathematical investigation is necessary to

assess the implications of such simplifications. Take, for example, the electrostatic potential of a device. Physically, we know that such a potential exists. Hence, a sound model should guarantee its existence – also from a mathematical point of view. If the existence cannot be shown, then the model does not represent the physical world accurately. Apart from existence, uniqueness of the solution is often desirable as well as continuous dependence on the initial data.

The mathematical technique used to prove existence and uniqueness depends on the device geometry and the model. The first existence result of the van Roosbroeck system was shown by Mock [32]. Since then several results have been obtained by Gajewski and Gröger, we refer the interested reader to [33, 34]. In [34], the key tool to show the existence and uniqueness of the time dependent system is based on finding a Lyapunov function. Moreover, Gajewski and Gröger presented the first result which considered Fermi-Dirac statistics instead of Boltzmann statistics. There are other important existence results. We would like to mention explicitly the results studied by Markowich see for example [35], Jüngel [36], and Jerome [37].

We would like to show the reader that these results are not of purely analytical interest but can also be used to design numerical methods. Gummel's method [38], for example, (see Section 5) is based on the same fixed point iteration technique used to obtain the existence result which we discuss next. The connection to numerics can be found in [37]. We would like to give the reader an idea regarding the proof of a standard result without going into the tricky details. We follow ideas from Markowich's textbook [39].

We consider the stationary van Roosbroeck system with Boltzmann statistics. Using a scaling that can be found in [39, Section 2.4] and making a change of variables, we can rewrite the steady-state van Roosbroeck system in the following way

$$-\lambda^2 \Delta \psi = \delta^2 e^{-\psi} v - \delta^2 e^{\psi} u + C, \tag{38a}$$

$$\nabla \cdot (\mu_n e^{\psi} \nabla u) = \tilde{R}, \tag{38b}$$

$$\nabla \cdot (\mu_p e^{-\psi} \nabla v) = \tilde{R}. \tag{38c}$$

The densities n and p are related to the so-called *Slotboom variables* u and v via $n = \delta^2 e^{\psi} u$ and $p = \delta^2 e^{-\psi} v$. In (38), the parameter λ denotes the normed characteristic Debye length of the device, δ^2 indicates the scaled intrinsic carrier density and $\tilde{R}$ is the scaled recombination term. It is of the form $\tilde{R} = c(\psi, u, v)(uv - 1)$ with $c(\psi, u, v) > 0$. The chosen scaling and change of variables make it possible to rewrite the boundary conditions. We consider only Ohmic contacts and homogeneous Neumann boundaries.

In order to prove the existence of solutions for the system (38) equipped with suitable boundary conditions, we need to make several technical assumptions. We refer the interested reader to [39] where these assumptions are well explained as well as physically and mathematically justified. Here, we would rather like to focus on the key idea of the proof which is exploited numerically, omitting mathematical detail. The existence proof is based on an iteration scheme which considers the Poisson equation (38a) decoupled from the continuity equations (38b) and (38c). The proof consists of the following steps:

1. We fix some $u_0, v_0 > 0$, and consider the semilinear elliptic problem

$$-\lambda^2 \Delta \psi = \delta^2 e^{-\psi} v_0 - \delta^2 e^{\psi} u_0 + C, \text{ in } \Omega, \qquad \text{(plus BC for } \psi \text{ on } \partial\Omega). \tag{39}$$

Using standard analytical results for semilinear elliptic equations (namely the Leray-Schauder's fixed point theorem and the maximum principle [40]) we prove that there exists a unique solution of the problem (39) that we denote with ψ_1.

2. We insert the solution ψ_1 of (39) into the decoupled linear elliptic equations

$$\nabla \cdot (\mu_n e^{\psi_1} \nabla u) = c(\psi_1, u_0, v_0)(uv_0 - 1), \text{ in } \Omega, \qquad \text{(plus BC for } u \text{ on } \partial\Omega), \qquad (40)$$

$$\nabla \cdot (\mu_p e^{-\psi_1} \nabla v) = c(\psi_1, u_0, v_0)(u_0 v - 1), \text{ in } \Omega, \qquad \text{(plus BC for } v \text{ on } \partial\Omega). \qquad (41)$$

We point out that in the right-hand side of (40) the rate c depends only on ψ_1 determined from the previous step and on the fixed u_0, v_0. The other term, $uv_0 - 1$, depends linearly on the unknown u. Analogous considerations are valid for (41). Physically, this means that in the factor describing relaxation to equilibrium, $uv - 1$, we freeze the hole density, more precisely the Slotboom variable v_0, in the continuity equation for the electrons and vice versa. Thanks to the non-negativity of $c(\psi_1, u, v)$ there exist unique solutions u_1 and v_1 to (40) and (41). This is ensured by standard results on linear elliptic equations (see for example [40]).

3. Based on the first two steps, we can now define a map H which maps (u_0, v_0) onto (u_1, v_1). This map is known as *Gummel map*. It is possible to prove that this map has a fixed point (u^*, v^*) which determines a (weak) solution (ψ^*, u^*, v^*) of the coupled system (38). The electrostatic potential ψ^* which solves Poisson's equation (38a) can be determined using the first step by substituting (u_0, v_0) with (u^*, v^*).

Finally, we discuss the uniqueness of solutions to the van Roosbroeck system. It is well known that for the steady-state system the uniqueness of the solution cannot be shown without additional assumptions, for example, on the applied voltage. This is no surprise, as in fact, some semiconductor devices (e.g. thyristors [41]) are designed to have multiple steady states. However, for a device in thermal equilibrium (see Section 3.1), we have $u = v = 1$. In this case, there is a unique function which satisfies the Poisson equation (38a). Hence, the solution $(\psi_e, 1, 1)$ is the unique equilibrium solution of the system (38), see [32]. For sufficiently small bias voltages the uniqueness of the solution is shown in [39] under some specific assumptions on the recombination rates. All recombination mechanisms appearing in Figurefulfill these assumptions. However, impact ionization rates for example are excluded.

3.5   Maximum principle

An important mathematical tool, often used for proofs similar to the ones in the previous section, is the maximum principle. Intuitively, the maximum principle states that if the domain is bounded and the right-hand side of the elliptic equation is positive, then the maximum of the solution is attained on the boundary of the domain [40].

4   Discretizing the van Roosbroeck system

In this section, we introduce a method for discretizing the van Roosbroeck system which is close to the physicist's approach to derive partial differential equations based on a subdivision of the computational domain into *representative elementary volumes* or *control volumes* . The *two-point flux* finite volume method described here can be seen as a straightforward generalization, preserving the properties of the one-dimensional Scharfetter-Gummel scheme in higher dimensions. Figure 10 shows a 2D simulation. The 2D variant of this approach was introduced as *box method* in [12]. Historically,
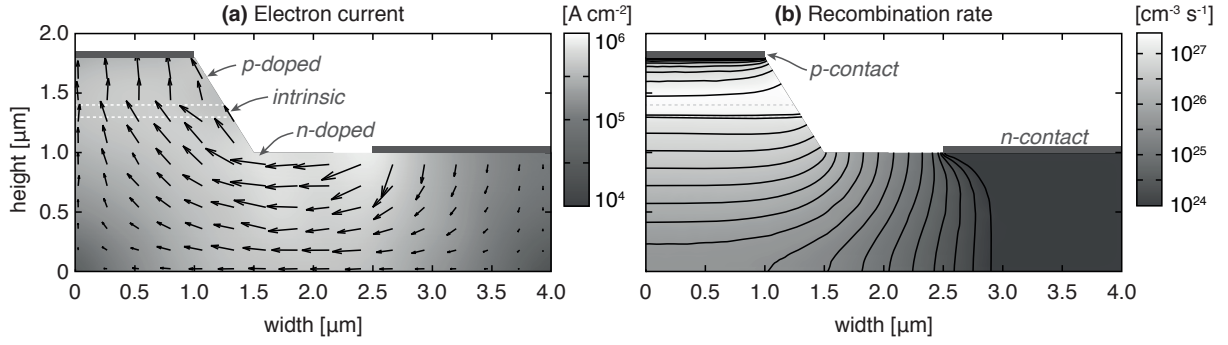
Figure 10: Exemplary results of a 2D simulation. The example is inspired by a ridge-waveguide laser with Ohmic contacts on the top of a mesa and at the side. For simplicity we restrict to a homogeneous material which is here GaAs with the parameters as given in Figure 2. Within the mesa an intrinsic domain is enclosed by a p-doped top-layer ($N_A = 2 \times 10^{18}\,\mathrm{cm}^{-3}$) and the n-doped substrate ($N_D = 2 \times 10^{18}\,\mathrm{cm}^{-3}$). The boundaries of the doped domains are shown in the pictures as dashed lines. (a) At an applied voltage of $1.5\,\mathrm{V}$ (flat band conditions) a significant electron current flow can be observed. The absolute value of the current density is shown by the gray scale, the arrows indicate the direction of particle flow (in the case of electrons the current density vector points in the opposite direction). (b) Plot of the total recombination rate at the same bias. The maximal recombination rate is observed in the vicinity of the intrinsic domain.
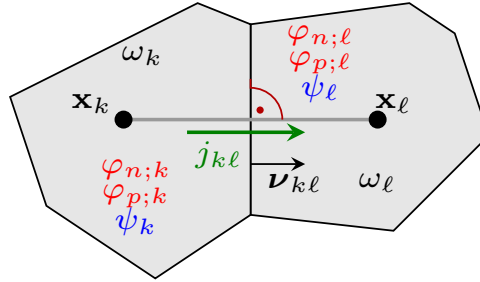

Figure 11: Two adjacent control volumes ω_k and ω_ℓ with corresponding data.

it goes back to [42]. The 3D variant of this method was probably first investigated in [43, 29].

The method has two main ingredients: a geometry based approach to obtain a system describing communicating control volumes and a consistent description of the fluxes between two adjacent control volumes. These will be discussed in the following two subsections. We finish this section by describing various properties of the finite volume scheme.

4.1   Finite volume method in higher dimensions

We partition the domain into N non-intersecting, convex polyhedral control volumes ω_k such that $\Omega = \bigcup_{k=1}^{N} \omega_k$. We associate with each control volume a node $\mathbf{x}_k \in \omega_k$. If the control volume intersects with the boundary of our domain, we demand that the node lies on the boundary $\mathbf{x}_k \in \partial\Omega \cap \omega_k$. We assume that the partition is *admissible* [44], that is the *edge* $\overline{\mathbf{x}_k \mathbf{x}_\ell}$ with length $h_{k\ell}$ is orthogonal to $\partial\omega_k \cap \partial\omega_\ell$. Thus, the normal vectors to $\partial\omega_k$ can be calculated by $\boldsymbol{\nu}_{k\ell} = (\mathbf{x}_\ell - \mathbf{x}_k)/\|\mathbf{x}_\ell - \mathbf{x}_k\|$. See Figure 11 for details.

The set of all nodes and control volumes is called the *mesh* of the domain Ω. For a discussion of constructive ways to obtain such mesh partitions, see Section 6. In order to keep the equations simple, we introduce two abbreviations,

$$\eta_n\left(\psi,\varphi_n\right) = \frac{q\left(\psi-\varphi_n\right)-E_c}{k_BT} \quad \text{and} \quad \eta_p\left(\psi,\varphi_p\right) = \frac{E_v - q\left(\psi-\varphi_n\right)}{k_BT},$$

and assume that we have only a single gate contact with gate voltage U_G. We integrate system (26) over ω_k and apply Gauss's divergence theorem, resulting in the integral equations

$$-\int_{\partial\omega_k} \varepsilon_s\nabla\psi\cdot\boldsymbol{v}ds + \int_{\partial\omega_k\cap\Gamma_G} \frac{\varepsilon_{\text{ox}}}{d_{\text{ox}}}(\psi-U_G)ds = q\int_{\omega_k}\left(C-N_c\mathscr{F}\left(\eta_n\left(\psi,\varphi_n\right)\right)+N_v\mathscr{F}\left(\eta_p\left(\psi,\varphi_p\right)\right)\right)d\mathbf{x}$$

$$-q\frac{\partial}{\partial t}\int_{\omega_k} N_c\mathscr{F}\left(\eta_n\left(\psi,\varphi_n\right)\right)d\mathbf{x} + \int_{\partial\omega_k}\mathbf{j}_n\cdot\boldsymbol{v}ds = q\int_{\omega_k}Rd\mathbf{x},$$

$$q\frac{\partial}{\partial t}\int_{\omega_k} N_v\mathscr{F}\left(\eta_p\left(\psi,\varphi_p\right)\right)d\mathbf{x} + \int_{\partial\omega_k}\mathbf{j}_p\cdot\boldsymbol{v}ds = -q\int_{\omega_k}Rd\mathbf{x},$$

for $k = 1,\ldots,N$. Here, $\boldsymbol{v}$ is outward-pointing unit normal to the control volume ω_k, see Figure 11. These equations represent an integral form of the van Roosbroeck system on every control volume. In particular, the first equation is Gauss' law of electrodynamics. The other two equations are balance laws for the carrier densities. The densities in each control volume change only due to in and outflow through the boundary or recombinative processes.

Next, the surface integrals are split into the sum of integrals over the planar interfaces between the control volume ω_k and its neighbors. Employing one point quadrature rules for the surface and volume integrals, we deduce the finite volume scheme

$$\sum_{\omega_\ell\in\mathscr{N}(\omega_k)} |\partial\omega_k\cap\partial\omega_\ell|D_{k,\ell} = q|\omega_k|\left(C-N_c\mathscr{F}\left(\eta_n\left(\psi_k,\varphi_{n;k}\right)\right)+N_v\mathscr{F}\left(\eta_p\left(\psi_k,\varphi_{p;k}\right)\right)\right)$$

$$+|\partial\omega_k\cap\Gamma_G|\frac{\varepsilon_{\text{ox}}}{d_{\text{ox}}}(U_G-\psi_k) \tag{42a}$$

$$-q|\omega_k|N_c\frac{d}{dt}\mathscr{F}\left(\eta_n\left(\psi_k,\varphi_{n;k}\right)\right) + \sum_{\omega_\ell\in\mathscr{N}(\omega_k)} |\partial\omega_k\cap\partial\omega_\ell|j_{n;k,\ell} = q|\omega_k|R_k, \tag{42b}$$

$$q|\omega_k|N_v\frac{d}{dt}\mathscr{F}\left(\eta_p\left(\psi_k,\varphi_{p;k}\right)\right) + \sum_{\omega_\ell\in\mathscr{N}(\omega_k)} |\partial\omega_k\cap\partial\omega_\ell|j_{p;k,\ell} = -q|\omega_k|R_k. \tag{42c}$$

In the above formulas, $\mathscr{N}(\omega_k)$ denotes the set of all control volumes neigboring ω_k. In 2D, the measure $|\partial\omega_k\cap\partial\omega_\ell|$ corresponds to the length of the boundary line segment and in 3D to the area of the intersection of the boundary surfaces. The measure $|\omega_k|$ is in 2D given by the area and in 3D by the volume of the control volume ω_k. The unknowns ψ_k, $\varphi_{n;k}$ and $\varphi_{p;k}$ are approximations of the electric potential as well as the quasi Fermi potentials for electrons and holes evaluated at node $\mathbf{x}_k$ like already introduced for the one-dimensional case in Section 2. Accordingly, R_k is defined as

$$R_k = R\left(N_c\mathscr{F}\left(\eta_n\left(\psi_k,\varphi_{n;k}\right)\right),N_v\mathscr{F}\left(\eta_p\left(\psi_k,\varphi_{p;k}\right)\right)\right).$$

The numerical fluxes $D_{k,\ell}$, $j_{n;k,\ell}$ and $j_{p;k,\ell}$ approximate $-\varepsilon\nabla\psi\cdot\boldsymbol{v}_{k\ell}$, $\mathbf{j}_n\cdot\boldsymbol{v}_{k\ell}$ and $\mathbf{j}_p\cdot\boldsymbol{v}_{k\ell}$, respectively, on the interfaces between two adjacent control volumes ω_k and ω_ℓ, see Figure 11. As in the 1D case, we assume that these fluxes can be expressed as nonlinear functions depending on the values $\psi_k,\varphi_{n;k},\varphi_{p;k}$ and $\psi_\ell,\varphi_{n;\ell},\varphi_{p;\ell}$.

The electric displacement flux is approximated by

$$D_{k,\ell} = -\varepsilon_s \frac{\psi_\ell - \psi_k}{h_{k,\ell}},$$

where

$$h_{k,\ell} = \|\mathbf{x}_\ell - \mathbf{x}_k\|$$

is the edge length, compare with (11).

For the Boltzmann approximation, the numerical charge carrier fluxes can be approximated via the Scharfetter-Gummel expression (17). In theory, any classical technique such as central differences or upwinding could be used to discretize the numerical fluxes. However, the former suffers from instability issues (as previously seen in Section 2.7) and neither scheme is consistent with the thermodynamic equilibrium. We will explain what this means in Section 4.3. In the next section we discuss thermodynamically consistent schemes for non-Boltzmann statistics.

The finite volume scheme (42) yields a nonlinear system of $3N$ equations depending on $3N$ variables. We can directly substitute Dirichlet boundary values in the equations. In practice, however, this way of handling Dirichlet values is very technical to implement. Exploiting floating point arithmetic, the Dirichlet penalty method [45] provides a reasonable alternative. Physically, it replaces the Dirichlet boundary conditions by gate boundary conditions with very high oxide permittivity.

4.2 Scharfetter-Gummel fluxes and their non-Boltzmann generalizations

In 1D, we have already discussed the highly effective flux discretization scheme proposed by Scharfetter and Gummel for Boltzmann statistics [11]. They derive the numerical flux by locally solving a linear two-point boundary value problem. The one-dimensional idea immediately carries over to higher dimensions if we insert the Scharfetter-Gummel flux (17) into the discrete system (42). However, if the Boltzmann approximation is not valid anymore, we can no longer derive the flux like Scharfetter and Gummel suggested.

This motivated the work in [46] where the Scharfetter-Gummel idea was generalized to a large class of nonlinear convection-diffusion problems, allowing to define consistent numerical fluxes from nonlinear two-point boundary value problems. Unfortunately, these *generalized Scharfetter-Gummel schemes* cannot be expressed by closed formulas. Sometimes, however, the local fluxes can be obtained iteratively [26]. It is also possible to approximate the two-point boundary value problems by simpler ones (for example by freezing some coefficients). This leads to *modified Scharfetter-Gummel schemes*. We will adress some of these schemes now.

For the sake of readability, we provide the formulas for electrons only. The formulas for holes follow similarly.

Generalized Scharfetter-Gummel schemes

By the construction of our mesh, it suffices to study the one-dimensional flux j_n along the edge $\overline{\mathbf{x}_k \mathbf{x}_\ell}$. For general distribution functions $\mathscr{F}$, we want to solve the ordinary differential equation

$$\frac{d}{dx} j_n = \frac{d}{dx} \left(-q\mu_n N_c \mathscr{F} \left(\eta_n \left(\psi, \varphi_n \right) \right) \nabla \varphi_n \right) = 0$$

on the interval $[0, h_{k,\ell}]$ with boundary conditions

$$\varphi_n(0) = \varphi_{n;k} \text{ and } \varphi_n\left(h_{k,\ell}\right) = \varphi_{n;\ell}$$

where $\varphi_{n;k}$ and $\varphi_{n,\ell}$ is the value of the quasi Fermi potential at the nodes $\mathbf{x}_k$ and $\mathbf{x}_\ell$, respectively, see Figure 11. We assume now that the flux is constant between both nodes and denote it with $j_{n;k,\ell}$. Integrating twice leads to an integral equation [26] for the unknown current, namely

$$\int_{\eta_{n;k}}^{\eta_{n;\ell}} \left(\frac{j_{n;k,l}/j_0}{\mathscr{F}(\eta)} + \frac{\psi_\ell - \psi_k}{U_T}\right)^{-1} d\eta = 1, \tag{43}$$

where $j_0 = q\mu_n N_c \dfrac{U_T}{h_{k,\ell}}$ and the limits are given by $\eta_{n;k} = \eta_n\left(\psi_k, \varphi_{n;k}\right)$ and $\eta_{n;\ell} = \eta_n\left(\psi_\ell, \varphi_{n;\ell}\right)$. For strictly monotonously increasing $\mathscr{F}(\eta)$ this equation has always a unique solution [47].

For the Boltzmann approximation $\mathscr{F}(\eta) = \exp(\eta)$ this integral equation can be solved analytically and yields the classical Scharfetter-Gummel expression for the flux (17). In [26] it was shown that for the Blakemore distribution function $\mathscr{F}\left(\eta\right) = \frac{1}{\exp(-\eta)+\gamma}$, the integral equation yields a fixed point equation

$$\widehat{j}_{n;k,\ell} = B\left(\gamma\widehat{j}_{n;k,\ell} + \frac{\psi_\ell - \psi_k}{U_T}\right)e^{\eta_{n;\ell}} - B\left(-\left[\gamma\widehat{j}_{n;k,\ell} + \frac{\psi_\ell - \psi_k}{U_T}\right]\right)e^{\eta_{n;k}} \tag{44}$$

for the non-dimensionalized edge current $\widehat{j}_{n;k,\ell} = j_{n;k,l}/j_0$. The right-hand side is a Scharfetter-Gummel expression where the argument of the Bernoulli function is shifted by $\gamma\widehat{j}_{n;k,\ell}$. Hence, this reduces to the classical Scharfetter-Gummel scheme for $\gamma = 0$.

Since the Bernoulli function is strictly decreasing, this fixed point equation possesses a unique solution $\widehat{j}_{n;k,\ell}$. If we want to use the flux given by (44) in the discrete system (42), we need to solve for the flux $\widehat{j}_{n;k,\ell}$ twice (once for electrons and once for holes) on each discretization edge $\overline{\mathbf{x}_k\mathbf{x}_\ell}$. A few Newton steps are sufficient to solve this equation iteratively.

Even though (44) is restricted to the Blakemore approximation, it provides a useful scheme in the context of organic semiconductors. There it arises naturally as a model for materials with δ-shaped density of states [10, 25], describing a single transport level, see Figures 8 and 9. This has been described in Section 3.2.

Unfortunately, for a general statistical distribution function, no corresponding equation has been derived so far. Therefore, in [47] it was proposed to use piecewise approximations of $\mathscr{F}$ by Blakemore type or rational approximations of Padé type in order to obtain piecewise integrable expression from the local boundary value problem.

Modified Scharfetter-Gummel schemes

Bessemoulin-Chatard [48] derived a finite volume scheme for convection-diffusion problems by averaging the nonlinear diffusion term appropriately. This idea was generalized to more general distribution functions in [49], introducing a logarithmic average of the nonlinear diffusion enhancement

$$g_{n;k,\ell} = \frac{\eta_{n;k} - \eta_{n;\ell}}{\log\mathscr{F}\left(\eta_{n;k}\right) - \log\mathscr{F}\left(\eta_{n;\ell}\right)}$$

along the discretization edge. Using the generalized Einstein relation (35), one immediately observes that the diffusion enhancement g can be seen as a modification factor of the thermal voltage U_T. Replacing U_T in the Scharfetter-Gummel expression (17) by $U_T^* = U_T g_{n;k,\ell}$, we deduce the following modified Scharfetter-Gummel scheme

$$j_{n;k,\ell} = -\frac{q\mu_n U_T}{h_{k,\ell}} g_{n;k,\ell} \left(N_c \mathscr{F}(\eta_{n;k}) B\left(-\frac{\psi_\ell - \psi_k}{U_T g_{n;k,\ell}}\right) - N_c \mathscr{F}(\eta_{n;\ell}) B\left(\frac{\psi_\ell - \psi_k}{U_T g_{n;k,\ell}}\right) \right), \quad (45)$$

approximating the current along the edge.

Previously, we have replaced the thermal voltage by a suitable average along the edge. Now, we want to approximate $\mathscr{F}(\eta)$ along the edge by an exponential (Boltzmann approximation) by modifying the density of states N_c accordingly, that is

$$N_c \mathscr{F}(\eta) \approx N_{c;k,\ell}^* \exp(\eta).$$

This choice makes it possible to use the original Scharfetter-Gummel flux (17) by replacing N_c with $N_{c;k,\ell}^*$. One choice for the modified density of states is

$$N_{c;k,\ell}^*(\eta^*) = N_c \frac{\mathscr{F}(\eta^*)}{\exp(\eta^*)},$$

where $\eta^* \in [\eta_k, \eta_\ell]$, assuming $\eta_k \le \eta_\ell$. In practice, we might consider taking the geometric average between $N_c(\eta_k)$ and $N_c(\eta_\ell)$, which leads to another modified Scharfetter-Gummel scheme:

$$j_{n;k,\ell} = -\frac{q\mu_n U_T}{h_{k,\ell}} N_c \sqrt{\frac{\mathscr{F}(\eta_{n;k})\mathscr{F}(\eta_{n;\ell})}{\exp(\eta_{n;k})\exp(\eta_{n;\ell})}} \left(B\left(-\frac{\psi_\ell - \psi_k}{U_T}\right) e^{\eta_{n;k}} - B\left(\frac{\psi_\ell - \psi_k}{U_T}\right) e^{\eta_{n;\ell}} \right). \quad (46)$$

The idea behind this scheme was introduced in [50] for the numerical solution of the generalized Nernst-Planck system which is similar to the van Roosbroeck system (26). A variant of this scheme for Fermi-Dirac statistics is described in [14, 51] and numerically implemented in the semiconductor device simulation package WIAS-TeSCA [52].

4.3 Flux expressions consistent with thermodynamic equilibrium

As introduced in Section 3.1, the currents of holes and electrons vanish in thermodynamic equilibrium when no bias is applied. If a numerical scheme for zero bias boundary conditions results into vanishing numerical fluxes, we call it *consistent with the thermodynamical equilibrium*. In practice, one can examine this consistency by checking whether $j_{n;k,\ell} = j_{p;k,\ell} = 0$ if $\varphi_{n;k} = \varphi_{n;\ell}$ and $\varphi_{p;k} = \varphi_{p;\ell}$. Violating this property causes unphysical dissipation (spurious Joule heating) in the steady state attained for zero bias boundary conditions, which by definition is supposed to be the thermodynamic equilibrium [48].

All schemes introduced in Section 4.2 are consistent with the thermodynamical equilibrium. Indeed, let us assume that the quasi Fermi potentials φ_n and φ_p between two adjacent control volumes ω_k and ω_ℓ are equal. The consistency of the classical Scharfetter-Gummel (17) and the scheme using a modified density of states (46) are obvious since the Bernoulli function satisfies $B(-x) = \exp(x)B(x)$.

Due to the definition from the solution of the two-point boundary value problem, the generalized Scharfetter-Gummel scheme defined in (43) and its specialization for the

Blakemore approximation (44) are consistent with the thermodynamic equilibrium. And finally, the logarithmic average of the diffusion enhancement is the only possible average wich guarantees consistency with thermodynamic in the scheme (45). For details see [26, 47, 49].

4.4 Free energy and dissipation rate

For Boltzmann statistics it is rather straightforward to define discrete analoga of the free energy (36) and the dissipation rate (37). The positivity of the disrete dissipation rate was shown in [29], and the exponential decay of the free energy to its equilibrium value was proven in [53]. An overview of the entropy method for finite volume schemes has been given in [54]. First results on more general statistics functions in this respect have been obtained in [55].

These pioneering works strongly indicate that the choosen discretization approach results in discrete models which are consistent with the structural assumptions of nonequilibrium thermodynamics. A full account of these issues in the context of general statistics functions remains an open research topic.

4.5 Existence, uniqueness and convergence

There are very few existence proofs for the solutions of the discretized system (42). For the Boltzmann approximation, Gärtner [56] proved that the discretized steady state system has a solution which becomes unique if a small bias is applied. A similar result for Fermi statistics has been obtained in [57].

A convergence theory for the finite volume scheme for the full discrete system (42) and general flux functions is still missing. However, practical experience and a number of results make its convergence plausible.

For example, in one space dimension, second order convergence in the discrete maximum norm for the Scharfetter-Gummel scheme has been shown in [19]. Under the assumption that second derivatives of the continuous solution exist, in [58] for moderately sized drift terms and two-dimensional, square grids, first order convergence for the simple upwind scheme (see e.g. [21]), and second order convergence for the exponential fitting scheme in the L_2-norm has been shown. Re-interpretations of the finite volume Scharfetter-Gummel scheme as a nonstandard finite element method allowed to obtain convergence estimates for Scharfetter-Gummel schemes on Delaunay grids (see Section 6) [59, 60]. For a general approach to the convergence theory of finite volume schemes, see [44]. In [46], weak convergence (no order estimate) for a generalization of the Scharfetter-Gummel scheme to nonlinear convection-diffusion problems has been shown. A convergence proof for a variant of the van Roosbroeck system discretized with the simple upwind scheme was given in [61].

4.6 Maximum principle

When applied to the drift-diffusion formulation, compared to various variants of the stabilized finite element method, the two-point flux finite volume scheme is outstanding in the sense that it guarantees positivity of densities and absense of unphysical oscillations [62, 63]. It allows to carry over the discussions of Section 2.7 to the higher dimensional case.

5 Nonlinear solvers

In Section 2, we have already briefly mentioned that we need to solve a nonlinear discrete system of the form

$$0 = \mathbf{F}(\boldsymbol{\psi}, \boldsymbol{\varphi}_n, \boldsymbol{\varphi}_p) := \begin{pmatrix} \mathbf{F}_1(\boldsymbol{\psi}, \boldsymbol{\varphi}_n, \boldsymbol{\varphi}_p) \\ \mathbf{F}_2(\boldsymbol{\psi}, \boldsymbol{\varphi}_n, \boldsymbol{\varphi}_p) \\ \mathbf{F}_3(\boldsymbol{\psi}, \boldsymbol{\varphi}_n, \boldsymbol{\varphi}_p) \end{pmatrix}.$$

Here, we discuss two ways to do this: Newton's method and *Gummel's iteration method* [38], which is different from the previously discussed Scharfetter-Gummel scheme.

5.1 Newton's method

Assuming that a good starting guess has been provided for example by following the ideas in Section 2.6, Newton's method constructs a new $(k+1)$th iterate from the kth by solving the linear system

$$\begin{pmatrix} \frac{\partial \mathbf{F}_1}{\partial \boldsymbol{\psi}} & \frac{\partial \mathbf{F}_1}{\partial \boldsymbol{\varphi}_n} & \frac{\partial \mathbf{F}_1}{\partial \boldsymbol{\varphi}_p} \\ \frac{\partial \mathbf{F}_2}{\partial \boldsymbol{\psi}} & \frac{\partial \mathbf{F}_2}{\partial \boldsymbol{\varphi}_n} & \frac{\partial \mathbf{F}_2}{\partial \boldsymbol{\varphi}_p} \\ \frac{\partial \mathbf{F}_3}{\partial \boldsymbol{\psi}} & \frac{\partial \mathbf{F}_3}{\partial \boldsymbol{\varphi}_n} & \frac{\partial \mathbf{F}_3}{\partial \boldsymbol{\varphi}_p} \end{pmatrix}^k \begin{pmatrix} \boldsymbol{\delta\psi}^k \\ \boldsymbol{\delta\varphi}_n^k \\ \boldsymbol{\delta\varphi}_p^k \end{pmatrix} = - \begin{pmatrix} \mathbf{F}_1(\boldsymbol{\psi}^k, \boldsymbol{\varphi}_n^k, \boldsymbol{\varphi}_p^k) \\ \mathbf{F}_2(\boldsymbol{\psi}^k, \boldsymbol{\varphi}_n^k, \boldsymbol{\varphi}_p^k) \\ \mathbf{F}_3(\boldsymbol{\psi}^k, \boldsymbol{\varphi}_n^k, \boldsymbol{\varphi}_p^k) \end{pmatrix} \tag{47}$$

for the update vector

$$\begin{pmatrix} \boldsymbol{\delta\psi}^k \\ \boldsymbol{\delta\varphi}_n^k \\ \boldsymbol{\delta\varphi}_p^k \end{pmatrix} := \begin{pmatrix} \boldsymbol{\psi}^{k+1} - \boldsymbol{\psi}^k \\ \boldsymbol{\varphi}_n^{k+1} - \boldsymbol{\varphi}_n^k \\ \boldsymbol{\varphi}_p^{k+1} - \boldsymbol{\varphi}_p^k \end{pmatrix}.$$

Then the new iterate is obtained by adding the previous vector to the update. The advantage of Newton's method is that it converges quadratically if the starting guess is sufficiently close to the solution [17]. This allows to obtain highly accurate discrete solutions at low additional cost. The major drawback is that it might converge very slowly or even fail to converge if the starting guess is too far from the actual solution. Damping – multiplying the update with a factor less than 1 – is known to increase the convergence region. Another remedy is parameter embedding where one slowly changes a parameter, always using the old solution as a new starting guess. We have already employed this embedding technique in Section 2.6 when gradually increasing the bias voltage in the solution procedure.

An important advantage of finite element and finite volume discretizations is the fact that they create only next-neighbor couplings in the discretized systems. The resulting linearized systems are therefore sparse, i.e. the maximum number of nonzero elements in a matrix row is bounded by a constant independent of the number of discretization cells, making it possible to use highly economic storage schemes. For 2D applications, one can usually solve the resulting sparse linear system (47) via sparse direct solvers such as PARDISO [64, 65, 66, 67] or UMFPACK [68, 69]. Direct solvers calculate a representation of the system matrix as a product of easily solvable lower and upper triangular matrices, which unfortunately are not anymore sparse, increasing memory consumption and computational time especially in large 3D applications. This fill-in phenomenon is avoided by preconditioned Krylov subspace methods [70], which compared to the direct solvers need significant effort in tuning and adaptation to the problem at hand.

5.2   Gummel's method

Gummel [38, 13] suggested decoupling the three equations in the van Roosbroeck system. He devised an iterative method at the continuous level, which for Boltzmann statistics and drift-diffusion form leads to alternating between solving linear differential equations for the electric potential as well as the charge carrier densities. Suppose one already knows the iterate (ψ^k, n^k, p^k). In order to obtain the electric potential at the new level, ψ^{k+1}, one solves

$$0 = -\frac{1}{q}\nabla\cdot\left(\varepsilon_s\nabla\psi^{k+1}\right) + \left(n^k + p^k\right)\left(\frac{\psi^{k+1} - \psi^k}{U_T}\right) + n^k - p^k - C.$$

This formulation is motivated by linearizing a fixed point problem which one obtains from the Poisson equation [13]. Once one has solved for the electrostatic potential at the new level, one can successively solve the continuity equations from

$$0 = \nabla\cdot\mathbf{j}_n(\psi^{k+1}, n^{k+1}) - qR(\psi^{k+1}, n^k, p^k)$$
$$0 = \nabla\cdot\mathbf{j}_p(\psi^{k+1}, p^{k+1}) + qR(\psi^{k+1}, n^{k+1}, p^k).$$

Gummel's method is known to have a larger convergence region and a slower asymptotic convergence rate compared to Newtons's method. Depending on the software environment chosen, it also may be easier to implement. Note that standard existence and uniqueness proofs for the van Roosbroeck system rely on a similar decoupling strategy, see Section 3.4.

6   Mesh generation for the finite volume method

While appearing to be just a technical footnote compared to the questions of modeling, analysis and discretization, mesh generation in reality is a hard problem which deserves special attention. We focus on methods to construct admissible subdivisions of the computational domain Ω as used in Section 4.

6.1   Boundary conforming Delaunay meshes on polyhedral domains

Assume a partition (triangulation in 2D, tetrahedralization in 3D) of the polyhedral domain $\Omega = \bigcup_{k=1}^{N_\Sigma}\Sigma_k$ into non-overlapping simplices Σ_k as it is commonly used for finite element methods [71]. We require that this simplicial partition of Ω has the *boundary conforming Delaunay property* [72]. For a triangulation of a two dimensional domain this property is equivalent to:

   (i) For any two triangles with a common edge, the sum of their respective angles opposite to that edge is less or equal to 180°.

   (ii) For any triangle sharing an edge with $\partial\Omega$, its angle opposite to that edge is less or equal to 90°.

For a given vertex $\mathbf{x}_i \in X$, the *Voronoi cell* around X is the set

$$V_i = \left\{\mathbf{x}\in\mathbb{R}^d : \|\mathbf{x} - \mathbf{x}_i\| < \|\mathbf{x} - \mathbf{x}_j\| \text{ for all } \mathbf{x}_j\in X \text{ with } \mathbf{x}_j\neq\mathbf{x}_i\right\}.$$
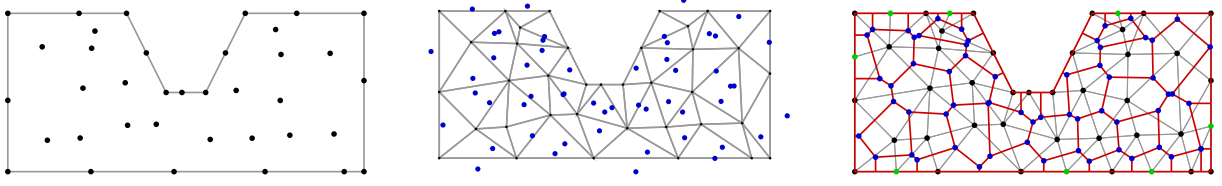
Figure 12: Left: Piecewise linear description of computational domain with given point cloud. Mid: Delaunay triangulation of domain and triangle circumcenters. As some boundary triangles have larger than 90° angles opposite to the boundary, their circumcenters (blue) are outside of the domain. Right: Boundary conforming Delaunay triangulation with automatically inserted additional points at the boundary (green), and Voronoi and restricted Voronoi cells (red). Created using triangle [73].

The *Voronoi diagram* – the set of Voronoi cells for all vertices in X – is dual to the *Delaunay triangulation* of the point set X in the sense that for each edge $\overline{\mathbf{x}_i \mathbf{x}_j}$ in the Delaunay triangulation, $\partial V_i \cap \partial V_j \neq \emptyset$. If the simplicial partition is boundary conforming Delaunay, the restricted Voronoi cells $\omega_i = \Omega \cap V_i$ are well defined and can be obtained by joining the circumcenters of the simplices adjacent to the vertex $\mathbf{x}_i$. These restricted Voronoi cells provide an admissible control volume partition as required in Section 4. We note that in order to implement the finite volume method as described in Section 4, there is no need for an explicit construction of the control volumina ω_i as geometrical objects. Given the simplical partition, it is sufficient to base the calculations on the simplicial contributions $s_{ij}^k = |\partial \omega_i \cap \partial \omega_j \cap \Sigma_k|$ and $|\omega_i \cap \Sigma_K|$, and to use a simplex based assembly loop like often done for finite elements [29]. Figure 12 shows (boundary conforming) Delaunay triangulations.

There are several efficient algorithms to construct Delaunay triangulations for a given point set X [74, 75]. These are good starting points of devising meshing algorithms in general. Many different problems complicate the generation of a mesh. For example, the boundary conforming Delaunay property is rather difficult to achieve, in particular it requires the careful insertion of additional points on the boundary. In 3D slivers (very flat tetrahedra) must be avoided. And lastly, it may be very complicated to fulfill additional requirements like constraints on the minimum angle or the local element size. Though there are still unsolved problems, the triangle ([73], 2D, free for non-commercial use) and TetGen ([76], 3D, open source) mesh generators help to create boundary conforming Delaunay meshes based on algorithms which are proven to deliver meshes with the desired properties in finite time for a broad class of geometries given by a piecewise linear description of the boundary.

Other mesh generation approaches, in particular the advancing front [77] and the octree method [78], are similarly widespread. However, while popular in finite element community, their design makes it much harder to use them as a starting point for generating boundary conforming Delaunay meshes.

6.2   Tensor product approaches

In simplified geometrical situations, rectangular and cuboid mesh structures are a straightforward way to generate admissible finite volume partitions of the computational domain [12]. Extrusion of a 2D boundary conforming Delaunay base mesh into a 3D mesh consisting of prisms (and optional subsequent subdivision of these prisms into tetrahe-

dra) provides another method to create admissible finite volume partitions [79].

6.3 Open problems

Charge densities and potentials in semiconductors exhibit interior and boundary layers, i. e. thin regions charaterized by rapid gradients in one direction and slow gradients in the orthogonal direction. This may happen in space charge regions in the vicinity of gate contacts and at p-n junctions. These layers and other possible "hotspots" due to recombination for example call for local mesh adaptation. Element size control via the mesh generators using a priori knowledge is often used in this situation [73, 76]. The development of reliable a posteriori mesh refinenment criteria is an open problem in the context of the strongly coupled van Roosbroeck system. A physically motivated heuristic approach based on the equidistribution of the dissipation rate was suggested in [29] and investigated in [80].

Mesh generation tools mostly fail to create boundary conforming Delaunay meshes which use thin, anisotropic simplices to resolve interior and boundary layers with an optimal number of points. A partial remedy in some situations can be provided by node offsetting [81], a technique still under development. In certain cases, tensor product approaches [79] give reasonable results.

7 Time discretization

In order to discretize the time derivative in the van Roosbroeck system (26), we define a series of discrete time values $0 = t_0, t_1, \ldots, t_M = T$ with step lengths $\tau^m = t^{m+1} - t^m$. We describe the temporal semi-discretization of the (spatially) continuous problem. For practical purposes it needs to be combined with the space discretization approach described in the previous sections. The implicit Euler time discretization scheme assumes given values $\psi^m, \varphi_n^m, \varphi_p^m, n^m, p^m$ of the variables at time t^m. Values at the subsequent time t^{m+1} are calculated by solving the nonlinear system of equations

$$-\nabla \cdot (\varepsilon_s \nabla \psi^{m+1}) = q(C - n^{m+1} + p^{m+1}) \tag{48a}$$

$$-q \frac{n^{m+1} - n^m}{\tau^m} - q\nabla \cdot \mu_n n^{m+1} \nabla \varphi_n^{m+1} = qR(n^{m+1}, p^{m+1}), \tag{48b}$$

$$q \frac{p^{m+1} - p^m}{\tau^m} - q\nabla \cdot \mu_p p^{m+1} \nabla \varphi_p^{m+1} = -qR(n^{m+1}, p^{m+1}) \tag{48c}$$

where

$$n^{m+1} = N_c \mathscr{F}(\eta_n(\psi^{m+1}, \varphi_n^{m+1}))$$
$$p^{m+1} = N_v \mathscr{F}(\eta_p(\psi^{m+1}, \varphi_p^{m+1}))$$

As a consequence, the nonlinear system (48), which is structurally similar to (42), has to be solved for each time step by iterative methods described in Section 5. An initial guess for these methods can be obtained from the old time step t^m or a linear extrapolation involving data from several previous time steps [82].

It is advisable to choose the size of the time steps τ^m according to multiple criteria, including the convergence radius of Newton's method, the free energy and local changes of the potentials.

At first glance, the computational cost of having to solve a nonlinear system for each time step appears to be rather high. However, this scheme is stable, independent of the the time step size and allows to carry over all advantages of the finite volume scheme from the stationary to the transient case. The transient discrete solution converges to the stationary one, in particular, for the corresponding boundary condition to the thermodynamic equilibrium solution. The free energy of the system decays during this approach to the equilibrium. In several cases, it has been proven that this decay is exponential [83, 55]. By preserving the physics, the implicit Euler scheme fits well to the thermodynamically motivated discretization schemes. The use of other schemes implies giving up some of these physical properties. If the resulting deviations from thermodynamic properties can be kept under control, higher order schemes (e.g. BDF methods [84]) might help to reduce computational costs due to a higher temporal convergence order.

Due to the perceived complexity and high computational costs of solving coupled nonlinear PDE systems, linear implicit methods, mixing linearization and time discretizations are considered as alternatives. Most prominent is the scheme devised in [85].

8   Contact terminal currents

In simulations one is usually interested in IV-curves, i.e. the dependency of terminal currents on applied voltages. Therefore, calculating terminal currents accurately is crucial to a successful postprocessing of the simulated field data. The *total current density* is given by

$$\mathbf{j} = \mathbf{j}_d + \mathbf{j}_n + \mathbf{j}_p$$

where $\mathbf{j}_d = -\varepsilon_s \nabla(\partial_t \psi) = \partial_t \mathbf{D}$ is the *displacement current density*. Taking the time derivative of the Poisson equation (26a) yields

$$-\nabla \cdot \varepsilon_s \nabla(\partial_t \psi) = q(\partial_t n - \partial_t p) = -\nabla \cdot \mathbf{j}_n - qR - \nabla \cdot \mathbf{j}_p + qR$$
$$\nabla \cdot \partial_t \mathbf{D} = -\nabla \cdot \mathbf{j}_n - \nabla \cdot \mathbf{j}_p$$

resulting in $\nabla \cdot \mathbf{j} = 0$, which physically implies charge conservation.

Given a set of contacts $\Gamma_\alpha \subset \partial\Omega$ for $\alpha = 1, \ldots, N_C$, the terminal current through contact α is defined as

$$I_\alpha = \int_{\Gamma_\alpha} \mathbf{j} \cdot v \, ds.$$

The correct calculation of this integral presupposes a regularity of the solution and its derivative which is not supported by analytical theory. Therefore, in [51, 52] a test function based technique was proposed which uses the weak formulation of the problem. For a physical motivation of this approach and an interpretation as a generalized Shockley-Ramo theorem we refer to [86]. For any α, let the function $T_\alpha \colon \Omega \to \mathbb{R}$ solve the boundary value problem

$$-\nabla^2 T_\alpha = 0 \qquad\qquad \text{in } \Omega, \tag{49}$$

$$\nabla T_\alpha \cdot n = 0 \qquad\qquad \text{on } \partial\Omega \setminus \bigcup_{\beta=1}^{N_C} \Gamma_\beta, \tag{50}$$

$$T_\alpha = \delta_{\alpha\beta} \qquad\qquad \text{on } \Gamma_\beta \text{ (for } \beta = 1, \ldots, N_C \text{ with } \beta \neq \alpha), \tag{51}$$

where $\delta_{\alpha\beta}$ denotes the Kronecker delta. As a consequence,

$$
\begin{aligned}
I_\alpha = \int_{\Gamma_\alpha} \mathbf{j} \cdot v \, ds &= \int_{\partial\Omega} T_\alpha \mathbf{j} \cdot v \, ds = \int_\Omega \nabla \cdot (T_\alpha \mathbf{j}) \, d\mathbf{x} \\
&= \int_\Omega \nabla T_\alpha \cdot \mathbf{j} \, d\mathbf{x} + \int_\Omega T_\alpha \nabla \cdot \mathbf{j} \, d\mathbf{x} \\
&= \int_\Omega \nabla T_\alpha \cdot (\mathbf{j}_n + \mathbf{j}_p) \, d\mathbf{x} + \partial_t \int_\Omega \nabla T_\alpha \cdot \mathbf{D} \, d\mathbf{x}
\end{aligned}
$$

Given the semi-discretization in time from Section 7, one arrives at

$$
I_\alpha^{m+1} = \int_\Omega \nabla T_\alpha \cdot (\mathbf{j}_n^{m+1} + \mathbf{j}_p^{m+1}) \, d\mathbf{x} + \frac{1}{\tau^m} \int_\Omega \nabla T_\alpha \cdot \left(\mathbf{D}^{m+1} - \mathbf{D}^m \right) \, d\mathbf{x}.
$$

Like in Section 4, we approximate equations (49)–(51) by a finite volume discretization. Using partial integration and the discretized terms derived in the previous sections we come up with an expression for the total current through the α-th contact

$$
I_\alpha^{m+1} \approx \sum_{\substack{\omega_\ell \in \mathcal{N}(\omega_k) \\ k < \ell}} |\partial\omega_k \cap \partial\omega_\ell| \left(j_{n;k,\ell}^{m+1} + j_{p;k,\ell}^{m+1} + \frac{D_{k,\ell}^{m+1} - D_{k,\ell}^m}{\tau^m} \right) (T_{\alpha;k} - T_{\alpha;\ell}). \tag{52}
$$

9 An alternative: the finite element method

We have put special emphasis on the finite volume method. However, it is worth pointing out that there are other approaches. The finite difference method which has been used to solve the van Roosbroeck system [13] on tensor product meshes is equivalent to the previously introduced finite volume method.

The most popular ansatz to deal with unstructured meshes is the finite element method [71]. It starts with a *weak formulation* of the steady-state van Roosbroeck problem (26). Each equation of the system is multiplied with a so-called test function and integrate in space. Integrating by parts, each equation of the steady-state system can be restated as the following problem:

$$
\text{find } u \in U \text{ such that } a(u,v) = f(v) \text{ for all } v \in V,
$$

where U is a function space containing the ansatz functions u and V a function space containing the test functions v. The map $a : U \times V \to \mathbb{R}$ has the structure

$$
a(u,v) = \int_\Omega \alpha(u) \nabla u \cdot \nabla v \, d\mathbf{x} - \int_{\partial\Omega} \nabla u \cdot \mathbf{n} v \, ds \tag{53}
$$

and the functional $f : V \to \mathbb{R}$ is continuous. The idea of a finite element method is to approximate this continuous problem with a discrete version. We approximate the infinite dimensional spaces U and V with finite dimensional subspaces U_h and V_h spanned by basis functions with localized support. Then we obtain a finite dimensional version of (53), namely

$$
\text{find } u_h \in U_h \text{ such that } a_h(u_h, v_h) = f(v_h) \text{ for all } v_h \in V_h.
$$

As it is sufficient to fulfill this condition for finitely many localized basis functions in V_h, we obtain a sparse (containing many zeros) nonlinear system of equations for the basis coefficients of u_h, assuming we are able to calculate the integrals. One usually approximates these integrals by quadrature rules.

Auf der Maur [87] suggested to write the van Roosbroeck system in this framework, using the quasi Fermi potential formulation of the flux. In this case one has

$$a^{\psi}(\psi, v) = \int_{\Omega} \varepsilon_s \nabla \psi \cdot \nabla v \, d\mathbf{x} + \int_{\Gamma_G} \frac{\varepsilon_{\text{ox}}}{d_{\text{ox}}} (\psi - U_G) v \, ds, \quad f^{\psi}(v) = q \int_{\Omega} (p - n + C) v \, d\mathbf{x}, \quad (54a)$$

$$a^{\varphi_n}(\varphi_n, v) = \int_{\Omega} \mu_n n \nabla \varphi_n \cdot \nabla v \, d\mathbf{x}, \qquad\qquad f^{\varphi_n}(v) = \int_{\Omega} R v \, d\mathbf{x}, \qquad (54b)$$

$$a^{\varphi_p}(\varphi_p, v) = \int_{\Omega} \mu_p p \nabla \varphi_p \cdot \nabla v \, d\mathbf{x}, \qquad\qquad f^{\varphi_p}(v) = \int_{\Omega} R v \, d\mathbf{x}. \qquad (54c)$$

At the Dirichlet parts of the boundary, namely at the Ohmic contacts $\Gamma_{O,\alpha}$ introduced in Section 3, we assume that test functions v vanish and the ansatz functions denoted by ψ, φ_n and φ_p fulfill the the Dirchlet boundary conditions (28). Note, that the gate boundary conditions (29) have been incorparated into the boundary part of the quadratic form (54a).

We point out that for Poisson's equation $\alpha^{\psi}(\psi) = \varepsilon_s$ and for the continuity equations we have $\alpha^{\varphi_n}(\varphi_n) = \mu_n n$ and $\alpha^{\varphi_p}(\varphi_p) = \mu_p p$, respectively. Due to the formulation of problem with quasi Fermi potentials as unknowns, this means that $\alpha^{\varphi_n}(\varphi_n)$ and $\alpha^{\varphi_p}(\varphi_p)$ introduce nonlinearities in a^{φ_n} and a^{φ_p}. The integrals on the left-hand side of (54) have no analytical expressions and are approximated using quadrature rules [71].

Essential for this finite element scheme is the underlying potential-based formulation of the flux in terms of φ_n and φ_p. If one attempts to apply the finite element method using the density-based, drift-diffusion formulation of the flux, one encounters a lot of technical difficulties and one has to stabilize the finite element method [62, 88]. A convergence proof of the finite element method for a similar system in a somewhat different context (and without recombination) is available in [89].

10 Extensions and outlook

In this chapter, we discussed the most important numerical solution techniques of the van Roosbroeck system, describing the transport of electrons and holes in semiconductors in a self-consistent electric field. This approach provides the core functionalities for a solver which can be enhanced by models describing additional physical phenomena and more complex device structures including for example heterostructures. We mention a number of additional extensions and point to the corresponding literature.

Additional physical models

Many devices require a more accurate description of the carrier mobilities. For example, models of ionized impurity scattering, high-field drift velocity saturation and similar effects [13, 90] introduce dependencies of the mobilties on carrier densities and the electric field strength, resulting in even more nonlinear couplings in the system.

The carrier transport in organic semiconductors is governed by hopping transport between the energy states of neighboring molecules. The van Roosbroeck system can

be used to describe this effectively [8, 27]. This may require the use of statistical distribution functions which reflect the distribution of the energy transport levels such as Blakemore for δ-shaped densities of states or Gauß-Fermi [10]. In this context, the correct treatmeant of the diffusion enhancement is vital. One also has to account for the nonlinear mobilities [8, 91] related to the energetic disorder characteristic for organic semiconductors.

Spin-polarized drift diffusion models have been proposed in [92] for the description of spintronic devices. They generalize the van Roosbroeck system, introducing spin-resolved densities for electron and holes and additional mechanisms describing the spin relaxation. They have been recently studied also from a numerical point of view in [93, 94, 95].

Coupling the van Roosbroeck system to other models

When modeling lasers one has to couple the van Roosbroeck system to equations for the optical modes. This introduces additional recombination processes, describing the stimulated emission. Additionally, one has to consider balance equations for the photon number. A comprehensive model (also including heating effects) along with a numerical solution strategy is given in [14].

In semiconductor devices with embedded nanostructures (such as quantum dots and quantum wells), one has to couple the drift diffusion equations to equations describing the dynamics of the carriers localized in the nanostructures [4, 5, 7]. A multiscale approach for coupling atomistic with continuum drift-diffusion models is presented in [96].

If heating effects become important, the van Roosbroeck system needs to be extended by an energy transport model for the heat flow in the device. For a thermodynamically consistent extension of the van Roosbroeck system to account for this effect we refer to [14, 31].

Methods for doping optimization

An important task when designing semiconductor devices is finding a suitable doping profile. This is an analytical and numerical challenge. Electric properties of the device can be improved by optimizing the doping profiles using suitable objective functionals [97, 98, 99]. Recently, the approach introduced in [97] has been extented for the optimization of doping profiles in lasers [100].

Alternative modeling approaches for carrier transport

The van Roosbroeck uses implicitly the assumption that the carrier ensemble is locally in quasi equilibrium. When this assumption is not met, for example, for hot electrons, one has to consider alternative approaches. The most common ones are: hydrodynamic models [101] and approximations of the Boltzmann equation which are derived from a spherical harmonics expansion [102]. The book [103] gives a mathematically oriented overview of these topics.

Acknowledgments

References

[1] W. Van Roosbroeck. Theory of the flow of electrons and holes in germanium and other semiconductors. *Bell System Technical Journal*, 29(4):560–607, Oct 1950.

[2] S. M. Sze and K. K. Ng. *Physics of Semiconductor Devices*. Wiley, 3rd edition, November 2006. ISBN: 978-0-471-14323-9.

[3] J. Piprek. *Optoelectronic Devices: Advanced Simulation and Analysis*. Springer, 2005.

[4] M. Grupen and K. Hess. Simulation of carrier transport and nonlinearities in quantum-well laser diodes. *IEEE J. Quantum Electron.*, 34(1):120–140, 1998.

[5] S. Steiger, R. G. Veprek, and B. Witzigmann. Unified simulation of transport and luminescence in optoelectronic nanostructure. *J. Comput. Electron.*, 7(4):509–520, 2008.

[6] Th. Koprucki, H.-C. Kaiser, and J. Fuhrmann. Electronic states in semiconductor nanostructures and upscaling to semi-classical models. In Alexander Mielke, editor, *Analysis, Modeling and Simulation of Multiscale Problems*, pages 365–394. Springer Berlin Heidelberg, 2006.

[7] Th. Koprucki, A. Wilms, A. Knorr, and U. Bandelow. Modeling of quantum dot lasers with microscopic treatment of Coulomb effects. *Opt. Quant. Electron.*, 42:777–783, 2011.

[8] R. Coehoorn, W. F. Pasveer, P. A. Bobbert, and M. A. J. Michels. Charge-carrier concentration dependence of the hopping mobility in organic materials with Gaussian disorder. *Phys. Rev. B*, 72(15):155206, Oct 2005.

[9] S. L. M. van Mensfoort and R. Coehoorn. Effect of Gaussian disorder on the voltage dependence of the current density in sandwich-type devices based on organic semiconductors. *Physical Review B*, 78(8), Aug 2008.

[10] G. Paasch and S. Scheinert. Charge carrier density of organics with Gaussian density of states: Analytical approximation for the Gauss-Fermi integral. *J. Appl. Phys.*, 107(10):104501, 2010.

[11] D. L. Scharfetter and H. K. Gummel. Large-signal analysis of a silicon read diode oscillator. *IEEE Transactions on Electron Devices*, 16(1):64–77, Jan 1969.

[12] W. Fichtner, D. J. Rose, and R. E. Bank. Semiconductor device simulation. *SIAM Journal on Scientific and Statistical Computing*, 4(3):391–415, 1983.

[13] S. Selberherr. *Analysis and simulation of semiconductor devices*. Springer, Wien, New York, 1984.

[14] U. Bandelow, H. Gajewski, and R. Hünlich. Fabry–Perot Lasers: Thermodynamics-Based Modeling. In Joachim Piprek, editor, *Optoelectronic Devices*. Springer, 2005.

[15] A. Mielke. A gradient structure for reaction-diffusion systems and for energy-drift-diffusion systems. *Nonlinearity*, 24(4):1329, 2011.

[16] S. R. de Groot and P. Mazur. *Non-equilibrium thermodynamics*. North Holland, 1962.

[17] P. Deuflhard. *Newton methods for nonlinear problems: affine invariance and adaptive algorithms*, volume 35. Springer, 2011.

[18] D. N. Allen and R. V. Southwell. Relaxation methods applied to determine the motion, in two dimensions, of a viscous fluid past a fixed cylinder. *Quart. J. Mech. and Appl. Math.*, 8:129–145, 1955.

[19] A. M. Il'in. A difference scheme for a differential equation with a small parameter multiplying the second derivative. *Mat. zametki*, 6:237–248, 1969.

[20] J.S. Chang and G. Cooper. A practical difference scheme for Fokker-Planck equations. *Journal of Computational Physics*, 6(1):1–16, 1970.

[21] H.-G. Roos, M. Stynes, and L. Tobiska. *Robust numerical methods for singularly perturbed differential equations*, volume 24. Springe, 2008.

[22] K. W. Morton. *Numerical Solution Of Convection-Diffusion Problems*. Applied Mathematics. Taylor & Francis, 1996.

[23] S. Yu. Karpov. *Visible Light-Emitting Diodes*, chapter 14, pages 303–325. Wiley-VCH Verlag GmbH & Co. KGaA, Weinheim, Germany, 2007.

[24] J. S. Blakemore. The Parameters of Partially Degenerate Semiconductors. *Proc. Phys. Soc. London A*, 65:460–461, 1952.

[25] M. Gruber, E. Zojer, F. Schürrer, and K. Zojer. Impact of materials versus geometric parameters on the contact resistance in organic thin-film transistors. *Advanced Functional Materials*, 23(23):2941–2952, 2013.

[26] Th. Koprucki and K. Gärtner. Discretization scheme for drift-diffusion equations with strong diffusion enhancement. *Opt. Quant. Electron.*, 45(7):791–796, 2013.

[27] S. L. M. van Mensfoort and R. Coehoorn. Effect of Gaussian disorder on the voltage dependence of the current density in sandwich-type devices based on organic semiconductors. *Phys. Rev. B*, 78(8):085207, Aug 2008.

[28] R. Haase. *Thermodynamics of irreversible processes*. Addison-Wesley, 1968.

[29] H. Gajewski and K. Gärtner. On the discretization of van Roosbroeck's equations with magnetic field. *Z. Angew. Math. Mech.*, 76(5):247–264, 1996.

[30] H. Gajewski and K. Gröger. Semiconductor equations for variable mobilities based on Boltzmann statistics or Fermi-Dirac statistics. *Math. Nachr.*, 140(1):7–36, 1989.

[31] G. Albinus, H. Gajewski, and R. Hünlich. Thermodynamic design of energy models of semiconductor devices. *Nonlinearity*, 15(2):367, 2002.

[32] M. S. Mock. On equations describing steady-state carrier distributions in a semiconductor device. *Comm. Pure Appl. Math.*, 25(25):781–792, 1972.

[33] H. Gajewski and K. Gröger. On the basic equations for carrier transport in semiconductors. *Journal of Mathematical Analysis and Applications*, 113:12–35, 1986.

[34] H. Gajewski. On existence, uniqueness and asymptotic behavior of solutions of the basic equations for carrier transport in semiconductors. *Z. Angew. Math. Mech. 65*, 2:101–108, 1985.

[35] P. A. Markowich. A nonlinear eigenvalue problem modelling the avalanche effect in semiconductor diodes. *SIAM J. Math. Anal.*, 6:1268–1283, 1985.

[36] A. Jüngel. On the existence and uniqueness of transient solutions of a degenerate nonlinear drift-diffusion model for semiconductors. *Math. Models Methods Appl. Sci.*, 04:677, 1994.

[37] J. W. Jerome. *Analysis of Charge Transport. A Mathematical Study of Semiconductor Devices*. Springer, Berlin Heidelberg, 1996.

[38] H. K. Gummel. A self-consistent iterative scheme for one-dimensional steady state transistor calculations. *Electron Devices, IEEE Transactions on*, 11(10):455–465, Oct 1964.

[39] P. A. Markowich. *The Stationary Semiconductor Device Equations*. Springer-Verlag Wien New York, 1986.

[40] D. Gilbarg and N. S. Trudinger. *Elliptic Partial Differential Equations of Second Order*. Classics in Mathematics. Springer, Berlin, 2001. Reprint of the 1998 edition.

[41] I. Rubinstein. *Electro-diffusion of ions*, volume 11. SIAM, 1990.

[42] R. H. Macneal. An asymmetrical finite difference network. *Quart. Math. Appl.*, 11:295–310, 1953.

[43] P. Fleischmann and S. Selberherr. Three-dimensional Delaunay mesh generation using a modified advancing front approach. In *Proceedings of IMR97*, pages 267–278, 1997.

[44] R. Eymard, Th. Gallouët, and R. Herbin. Finite volume methods. *Handbook of numerical analysis*, 7:713–1018, 2000.

[45] J. W. Barrett and Ch. M. Elliott. Finite element approximation of the Dirichlet problem using the boundary penalty method. *Numerische Mathematik*, 49(4):343–366, 1986.

[46] R. Eymard, J. Fuhrmann, and K. Gärtner. A finite volume scheme for nonlinear parabolic equations derived from one-dimensional local Dirichlet problems. *Numerische Mathematik*, 102(3):463–495, 2006.

[47] K. Gärtner. Existence of bounded discrete steady state solutions of the van Roosbroeck system with monotone Fermi-Dirac statistic functions. *J. Comput. Electron.*, 14(3):773–787, 2015.

[48] M. Bessemoulin-Chatard. A finite volume scheme for convection–diffusion equations with nonlinear diffusion derived from the Scharfetter–Gummel scheme. *Numerische Mathematik*, 121(4):637–670, 2012.

[49] Th. Koprucki, N. Rotundo, P. Farrell, D. H. Doan, and J. Fuhrmann. On thermodynamic consistency of a Scharfetter–Gummel scheme based on a modified thermal voltage for drift-diffusion equations with diffusion enhancement. *Opt. Quant. Electron.*, 47(6):1327–1332, 2015.

[50] J. Fuhrmann. Comparison and numerical treatment of generalised Nernst-Planck models. *Computer Physics Communications*, 196:166 – 178, 2015.

[51] H. Gajewski. Analysis und Numerik von Ladungstransport in Halbleitern. *WIAS Report*, 0(6), 1993. ISSN 0942-9077.

[52] H. Gajewski, M. Liero, R. Nürnberg, and H. Stephan. WIAS-Tesca user manual 1.2. *WIAS Technical Report*, 0(14), 2016. ISSN: WIAS 1618-7776.

[53] A. Glitzky and K. Gärtner. Energy estimates for continuous and discretized electro-reaction–diffusion systems. *Nonlinear Analysis*, 70(2):788–805, 2009.

[54] C. Chainais-Hillairet. Entropy method and asymptotic behaviours of finite volume schemes. In J. Fuhrmann, M. Ohlberger, and Ch. Rohde, editors, *Finite Volumes for Complex Applications VII – Methods and Theoretical Aspects*, pages 17–35. Springer, 2014.

[55] M. Bessemoulin-Chatard and C. Chainais-Hillairet. Exponential decay of a finite volume scheme to the thermal equilibrium for drift–diffusion systems. *arXiv preprint arXiv:1601.00813*, 2016.

[56] K. Gärtner. Existence of Bounded Discrete Steady-State Solutions of the Van Roosbroeck System on Boundary Conforming Delaunay Grids. *SIAM Journal on Scientific Computing*, 31(2):1347–1362, jan 2009.

[57] K Gärtner. Existence of bounded discrete steady state solutions of the van Roosbroeck system with monotone Fermi-Dirac statistic functions. *J. Comput. Electron.*, 14(3):773–787, 2015.

[58] R. D. Lazarov, I.D. Mishev, and P. S. Vassilevski. Finite volume methods for convection-diffusion problems. *SIAM J. Numer. Anal.*, 33(1):31–55, 1996.

[59] J. J. H. Miller and S. Wang. An analysis of the Scharfetter-Gummel box method for the stationary semiconductor device equations. *RAIRO-Modélisation mathématique et analyse numérique*, 28(2):123–140, 1994.

[60] J. Xu and L. Zikatanov. A monotone finite element scheme for convection-diffusion equations. *Mathematics of Computation of the American Mathematical Society*, 68(228):1429–1446, 1999.

[61] C. Chainais-Hillairet, J.-G. Liu, and Y.-J. Peng. Finite volume scheme for multi-dimensional drift-diffusion equations and convergence analysis. *ESAIM: Mathematical Modelling and Numerical Analysis-Modélisation Mathématique et Analyse Numérique*, 37(2):319–338, 2003.

[62] R. E. Bank, W. M. Coughran Jr, and L. C. Cowsar. The finite volume scharfetter-gummel method for steady convection diffusion equations. *Computing and Visualization in Science*, 1(3):123–136, 1998.

[63] M. Augustin, A. Caiazzo, A. Fiebach, J. Fuhrmann, V. John, A. Linke, and R. Umla. An assessment of discretizations for convection-dominated convection-diffusion equations. *Comp. Meth. Appl. Mech. Engrg.*, 200:3395–3409, 2011.

[64] A. Kuzmin, M. Luisier, and O. Schenk. Fast methods for computing selected elements of the greens function in massively parallel nanoelectronic device simulations. In F. Wolf, B. Mohr, and D. Mey, editors, *Euro-Par 2013 Parallel Processing*, volume 8097 of *Lecture Notes in Computer Science*, pages 533–544. Springer Berlin Heidelberg, 2013.

[65] O. Schenk, M. Bollhöfer, and R. A. Römer. On large-scale diagonalization techniques for the anderson model of localization. *SIAM Rev.*, 50(1):91–112, February 2008.

[66] O. Schenk, A. Wächter, and M. Hagemann. Matching-based preprocessing algorithms to the solution of saddle-point problems in large-scale nonconvex interior-point optimization. *Computational Optimization and Applications*, 36(2-3):321–341, 2007.

[67] O. Schenk. PARDISO version 5.0.0. URL: http://www.pardiso-project.org. Accessed 2016-02-22.

[68] T. A. Davis. *Direct Methods for Sparse Linear Systems (Fundamentals of Algorithms 2)*. Society for Industrial and Applied Mathematics, Philadelphia, PA, USA, 2006.

[69] T. Davis. SuiteSparse version 4.5.1. URL: http://faculty.cse.tamu.edu/davis/suitesparse.html. Accessed 2016-02-22.

[70] Y. Saad. *Iterative methods for sparse linear systems*. Siam, 2003.

[71] P. Ciarlet. *The Finite Element Method for Elliptic Problems*. Society for Industrial and Applied Mathematics, 2002.

[72] H. Si, K. Gärtner, and J. Fuhrmann. Boundary conforming Delaunay mesh generation. *Computational Mathematics and Mathematical Physics*, 50(1):38–53, 2010.

[73] J. Shewchuk. Triangle: A two-dimensional quality mesh generator and Delaunay triangulator. URL: http://www.cs.cmu.edu/q̃uake/triangle.html. Accessed 2015-12-01.

[74] H. Edelsbrunner. *Algorithms in combinatorial geometry*. Springer-Verlag, Heidelberg, 1987.

[75] S.-W. Cheng, T. K. Dey, and J. R. Shewchuk. *Delaunay Mesh Generation*. Chapman & Hall/CRC, Boca Raton, FL, 1st edition, 2012.

[76] H. Si. TetGen version 1.5. URL: http://tetgen.org/. Accessed 2015-12-01.

[77] J. Schöberl. Netgen an advancing front 2d/3d-mesh generator based on abstract rules. *Computing and visualization in science*, 1(1):41–52, 1997.

[78] M. S. Shephard and M. K. Georges. Automatic three-dimensional mesh generation by the finite octree technique. *International Journal for Numerical methods in engineering*, 32(4):709–749, 1991.

[79] K. Gärtner and R. Richter. Depfet sensor design using an experimental 3d device simulator. *Nuclear Instruments and Methods in Physics Research Section A: Accelerators, Spectrometers, Detectors and Associated Equipment*, 568(1):12–17, 2006.

[80] B. Schmithüsen, K. Gärtner, and W. Fichtner. Grid adaptation for device simulation according to the dissipation rate. In *Simulation of Semiconductor Processes and Devices 1998*, pages 197–200. Springer, 1998.

[81] J. Krause, N. Strecker, and W. Fichtner. Boundary-sensitive mesh generation using an offsetting technique. *International Journal for Numerical Methods in Engineering*, 49(1-2):51–59, 2000.

[82] A. Fiebach, A. Glitzky, and A. Linke. Uniform global bounds for solutions of an implicit voronoi finite volume method for reaction–diffusion problems. *Numerische Mathematik*, 128(1):31–72, 2014.

[83] A. Glitzky. Exponential decay of the free energy for discretized electro-reaction–diffusion systems. *Nonlinearity*, 21(9):1989, 2008.

[84] E. Hairer, S. P. Norsett, and G. Wanner. *Solving Ordinary Differential Equations: Nonstiff problems. v. 2: Stiff and differential-algebraic problems*. Springer Verlag, 2010.

[85] M.S. Mock. A time-dependent numerical model of the insulated-gate field-effect transistor. *Solid-State Electronics*, 24(10):959–966, 1981.

[86] P. D. Yoder, K. Gärtner, U. Krumbein, and W. Fichtner. Optimized terminal current calculation for monte carlo device simulation. *IEEE Transactions on Computer-Aided Design of Integrated Circuits and Systems*, 16(10):1082–1087, 1997.

[87] M. Auf Der Maur. *A Multiscale Simulation Environment for Electronic and Optoelectronic Devices*. PhD thesis, University of Tor Vergata, 2008.

[88] V. John and P. Knobloch. On spurious oscillations at layers diminishing (SOLD) methods for convection–diffusion equations: Part I–A review. *Computer Methods in Applied Mechanics and Engineering*, 196(17):2197–2215, 2007.

[89] A. Prohl and M. Schmuck. Convergent discretizations for the Nernst-Planck-Poisson system. *Numerische Mathematik*, 111(4):591–630, 2009.

[90] V. Palankovski and R. Quay. *Analysis and Simulation of Heterostructure Devices*. Computational Microelectronics. Springer Science & Business Media, Vienna, 2004.

[91] H. Bässler. Charge transport in disordered organic photoconductors a monte carlo simulation study. *phys. stat. sol. (b)*, 175(1):15–56, 1993.

[92] J. Fabian, S.C. Erwin, et al. Bipolar spintronics: Fundamentals and applications. *IBM journal of research and development*, 50(1):121–139, 2006.

[93] A. Glitzky and K. Gärtner. Existence of bounded steady state solutions to spin-polarized drift-diffusion systems. *SIAM J. Math. Anal.*, 41(6):2489–2513, 2010.

[94] A. Jüngel, C. Negulescu, and P. Shpartko. Bounded weak solutions to a matrix drift-diffusion model for spin-coherent electron transport in semiconductors. *Mathematical Models and Methods in Applied Sciences*, 25(05):929–958, 2015.

[95] C. Chainais-Hillairet, A. Jüngel, and P. Shpartko. A finite-volume scheme for a spinorial matrix drift-diffusion model for semiconductors. *Numerical Methods for Partial Differential Equations*, 2015.

[96] M. Auf der Maur, A. Pecchia, G. Penazzi, F. Sacconi, and A. Carlo. Coupling atomistic and continuous media models for electronic device simulation. *J. Comput. Electron.*, 12(4):553–562, 2013.

[97] M. Hinze and R. Pinnau. An optimal control approach to semiconductor design. *Mathematical Models and Methods in Applied Sciences*, pages 89–107, 2002.

[98] M. Hinze and R. Pinnau. Second-order approach to optimal semiconductor design. *J Optim Theory Appl*, pages 179–199, 2007.

[99] M. Burger and R. Pinnau. Fast optimal design of semiconductor devices. *SIAM Journal on Applied Mathematics*, 64(1):108–126, 2003.

[100] D. Peschka, N. Rotundo, and M. Thomas. Towards doping optimization of semiconductor lasers. To appear in. *Journal of Computational and Theoretical Transport*, 2016.

[101] T. Grasser, Ting-Wei Tang, H. Kosina, and S. Selberherr. A review of hydrodynamic and energy-transport models for semiconductor device simulation. *Proceedings of the IEEE*, 91(2):251–274, 2003.

[102] S.-M. Hong and C. Jungemann. A fully coupled scheme for a Boltzmann-Poisson equation solver based on a spherical harmonics expansion. *J. Comput. Electron.*, 8(3):225–241, 2009.

[103] A. Jüngel. *Transport equations for semiconductors*, volume 773. Springer, 2009.